JGR Biogeosciences

RESEARCH ARTICLE
10.1029/2020JG006005

Key Points:

- Stoichiometric N:P-ratio imbalance increases ecosystem transpiration
- High nitrogen availability increases carbon uptake and changed the ecosystem from a carbon source to carbon neutral
- Ecosystem scale functional relationships are altered through nutrient availability and imbalance

Supporting Information:

Supporting Information may be found in the online version of this article.

Correspondence to:

T. S. El-Madany,
telmad@bgc-jena.mpg.de

Citation:

El-Madany, T. S., Reichstein, M., Carrara, A., Martín, M. P., Moreno, G., Gonzalez-Cascon, R., et al. (2021). How nitrogen and phosphorus availability change water use efficiency in a Mediterranean savanna ecosystem. *Journal of Geophysical Research: Biogeosciences*, *126*, e2020JG006005. https://doi.org/10.1029/2020JG006005

Received 11 AUG 2020
Accepted 3 MAR 2021

Author Contributions:

Conceptualization: Tarek S. El-Madany, Markus Reichstein, Mirco Migliavacca
Data curation: Tarek S. El-Madany, Arnaud Carrara, M. Pilar Martín, Gerardo Moreno, Rosario Gonzalez-Cascon, Vicente Burchard-Levine, Tiana W. Hammer, Olaf Kolle
Formal analysis: Tarek S. El-Madany, Thomas Wutzler, Mirco Migliavacca
Funding acquisition: Markus Reichstein, Mirco Migliavacca
Investigation: Tarek S. El-Madany, Arnaud Carrara, Mirco Migliavacca
Methodology: Tarek S. El-Madany, Thomas Wutzler, Mirco Migliavacca

How Nitrogen and Phosphorus Availability Change Water Use Efficiency in a Mediterranean Savanna Ecosystem

Tarek S. El-Madany[1], Markus Reichstein[1], Arnaud Carrara[2], M. Pilar Martín[3], Gerardo Moreno[4], Rosario Gonzalez-Cascon[5], Josep Peñuelas[6,7], David S. Ellsworth[8], Vicente Burchard-Levine[3], Tiana W. Hammer[1], Jürgen Knauer[1,9], Olaf Kolle[1], Yunpeng Luo[1], Javier Pacheco-Labrador[1], Jacob A. Nelson[1], Oscar Perez-Priego[1,10], Victor Rolo[4], Thomas Wutzler[1], and Mirco Migliavacca[1]

[1]Max Planck Institute for Biogeochemistry, Department Biogeochemical Integration, Jena, Germany, [2]Centro de Estudios Ambientales del Mediterráneo (CEAM), Charles R. Darwin 14, Spain, [3]Environmental Remote Sensing and Spectroscopy Laboratory (SpecLab), Spanish National Research Council, Madrid, Spain, [4]Forest Research Group, INDEHESA, University of Extremadura, Plasencia, Spain, [5]Department of Environment, National Institute for Agriculture and Food Research and Technology (INIA-CSIC), Madrid, Spain, [6]Global Ecology Unit CREAF-CSIC-UAB, Campus de Bellaterra (UAB) Edifici C, Catalonia, Spain, [7]CREAF, Campus de Bellaterra (UAB) Edifici C, Cerdanyola del Vallès, Catalonia, Spain, [8]Hawkesbury Institute for the Environment, Western Sydney University, Penrith, Australia, [9]CSIRO Oceans and Atmosphere, Canberra, Australia, [10]Department of Forest Engineering, ERSAF Research Group, University of Cordoba, Cordoba, Spain

Abstract Nutrient availability, especially of nitrogen (N) and phosphorus (P), is of major importance for every organism and at a larger scale for ecosystem functioning and productivity. Changes in nutrient availability and potential stoichiometric imbalance due to anthropogenic nitrogen deposition might lead to nutrient deficiency or alter ecosystem functioning in various ways. In this study, we present 6 years (2014–2020) of flux-, plant-, and remote sensing data from a large-scale nutrient manipulation experiment conducted in a Mediterranean savanna-type ecosystem with an emphasis on the effects of N and P treatments on ecosystem-scale water-use efficiency (WUE) and related mechanisms. Two plots were fertilized with N (NT, 16.9 Ha) and N + P (NPT, 21.5 Ha), and a third unfertilized plot served as a control (CT). Fertilization had a strong impact on leaf nutrient stoichiometry only within the herbaceous layer with increased leaf N in both fertilized treatments and increased leaf P in NPT. Following fertilization, WUE in NT and NPT increased during the peak of growing season. While gross primary productivity similarly increased in NT and NPT, transpiration and surface conductance increased more in NT than in NPT. The results show that the NPT plot with higher nutrient availability, but more balanced N:P leaf stoichiometry had the highest WUE. On average, higher N availability resulted in a 40% increased leaf area index (LAI) in both fertilized treatments in the spring. Increased LAI reduced aerodynamic conductance and thus evaporation at both fertilized plots in the spring. Despite reduced evaporation, annual evapotranspiration increased by 10% (48.6 ± 28.3 kg H_2O m^{-2}), in the NT plot, while NPT remained similar to CT (−1%, −6.7 ± 12.2 kgH_2O m^{-2}). Potential causes for increased transpiration at NT could be increased root biomass and thus higher water uptake or rhizosphere priming to increase P-mobilization through microbes. The annual net ecosystem exchange shifted from a carbon source in CT (75.0 ± 20.6 gC m^{-2}) to carbon-neutral in both fertilized treatments [−7.0 ± 18.5 gC m^{-2} (NT) 0.4 ± 22.6 gC m^{-2} (NPT)]. Our results show, that the N:P stoichiometric imbalance, resulting from N addition (without P), increases the WUE less than the addition of N + P, due to the strong increase in transpiration at NT, which indicates the importance of a balanced N and P content for WUE.

Plain Language Summary The availability of nutrients like nitrogen (N) and phosphorus (P) is important for every living organism on Earth. Due to human activities, especially combustion processes large amounts of N are transported into the atmosphere and ecosystems. Therefore, ecosystems receive additional N but no other nutrients. We are investigating if the addition of N alone will lead to deficits in other nutrients and thus impact the functioning of ecosystems. Hence, we set up a large-scale ecosystem experiment in a Mediterranean tree-grass ecosystem where we fertilized two plots with N (16.9 ha) and

Software: Jacob A. Nelson, Thomas Wutzler
Supervision: Markus Reichstein, Mirco Migliavacca
Validation: Tarek S. El-Madany
Visualization: Tarek S. El-Madany
Writing – original draft: Tarek S. El-Madany, Markus Reichstein, Arnaud Carrara, M. Pilar Martín, Gerardo Moreno, Rosario Gonzalez-Cascon, Josep Peñuelas, David S. Ellsworth, Jürgen Knauer, Yunpeng Luo, Javier Pacheco-Labrador, Oscar Perez-Priego, Victor Rolo, Thomas Wutzler, Mirco Migliavacca
Writing – review & editing: Tarek S. El-Madany, Markus Reichstein, Arnaud Carrara, M. Pilar Martín, Gerardo Moreno, Rosario Gonzalez-Cascon, Josep Peñuelas, David S. Ellsworth, Vicente Burchard-Levine, Tiana W. Hammer, Jürgen Knauer, Olaf Kolle, Yunpeng Luo, Javier Pacheco-Labrador, Jacob A. Nelson, Oscar Perez-Priego, Victor Rolo, Thomas Wutzler, Mirco Migliavacca

N + P (21.5 ha). A third plot served as the control treatment. While the N-only treatment created an imbalance between the available N and P, this imbalance was relieved in the N + P treatment where both N and P were provided. Our measurements showed that both fertilized treatments increased their carbon uptake and turned the ecosystem from a carbon source to carbon neutral. One of the main differences between the fertilized treatments which is associated with the imbalance of available N and P is the loss of water through the vegetation (transpiration). This increase in transpiration was only observed in the N-only but not in the N + P treatment. Our results show, that the N:P stoichiometric imbalance, resulting from N-only addition, increases the water-use efficiency (i.e., the carbon gain per water loss) less than the addition of N + P, due to the strong increase in transpiration at the N-only treatment.

1. Introduction

Nitrogen (N) and phosphorus (P) availability are key nutrient drivers of ecosystem carbon cycling (Coskun et al., 2016; Ellsworth et al., 2017; Fay et al., 2015; Fernández-Martínez et al., 2014; Jiang et al., 2019). Changes in nutrient availability can impact ecosystem function (Musavi et al., 2015; Reichstein et al., 2014), plant traits (Klodd et al., 2016; Liang et al., 2020; Maire et al., 2015), water-use efficiency (WUE) (Huang et al., 2015), and canopy structure (Migliavacca et al., 2017).

Current and projected levels of anthropogenic N deposition are expected to cause stoichiometric imbalances in plant-available N and P in several terrestrial ecosystems (Du et al., 2020; Peñuelas et al., 2010, 2013). In such a scenario, plants must adapt to altered and potentially imbalanced nutrient availability (Elser et al., 2010; Güsewell, 2004; Oldroyd & Leyser, 2020; Zhu et al., 2016). In terms of carbon and water fluxes, ecosystem-level responses due to nutrient availability and stoichiometric N:P imbalances are poorly understood and may differ from those at the leaf, plant, or community level, due to interactions and compensatory effects among and between plants and soil. At the ecosystem level, it is especially important to understand and characterize how resource-use efficiencies such as WUE are changing with the stoichiometric imbalance and climate change. Especially in semi-arid ecosystems, increases in WUE could have positive effects on carbon sequestration potential as more carbon can be fixed with the same limited amount of available water (Grunzweig et al., 2003). In addition, increased WUE allows for maintaining photosynthesis while losing less water through transpiration. This leads to less soil moisture depletion and avoids the earlier onset of water stress and senescence in summer (Luo et al., 2020). There is a physiological trade-off between nutrient-use efficiency and WUE (Field et al., 1983; Han et al., 2016) arising from the importance of stomatal openings in enhancing the former while decreasing the latter. However, it is unclear to what degree an imbalance of the N:P ratio at ecosystem level will influence transpiration and WUE or how it is regulated by climate variability (Fernández-Martínez et al., 2014; Jiang et al., 2019; Luyssaert et al., 2014; Peñuelas et al., 2010, 2013).

This knowledge gap owes to the small spatial scales of experiments that manipulate nutrient availability, which have typically ranged from individual leaves and plants in mesocosm experiments to the order of a few tens of meters in small plot studies (Fay et al., 2015; Ford et al., 2016; Wicklein et al., 2012). While these experiments provide answers for nutrient manipulations for specific ecosystem compartments, such as soil and plants, they do not allow for the quantification of ecosystem-scale responses by carbon and water fluxes or water-use efficiency (WUE) in an integrated system at high temporal resolutions. The reliability of previous ecosystem-scale studies of surface properties and N effects on ecosystem-atmosphere exchange has been widely debated. Many studies were based on natural spatial variability in N content and may be influenced by confounding factors, e.g., temperature, species, and stand density (de Vries et al., 2008; Luyssaert et al., 2014; Magnani et al., 2007, 2008). While studies concerning the relationship of leaf N and ecosystem functioning exist and can be improved upon, systematic studies of the role of P and N:P ratio imbalances at the ecosystem level are lacking (Du et al., 2020; Penuelas et al., 2020). In general, investigations of fluxes or resource-use efficiency at the ecosystem level, under controlled N and P nutrient treatments are missing.

This study aims to address these knowledge gaps and comprehensively quantify the effects of concomitant increasing N availability and increasing N:P imbalance on ecosystem functioning and on WUE in a semi-arid tree-grass ecosystem.

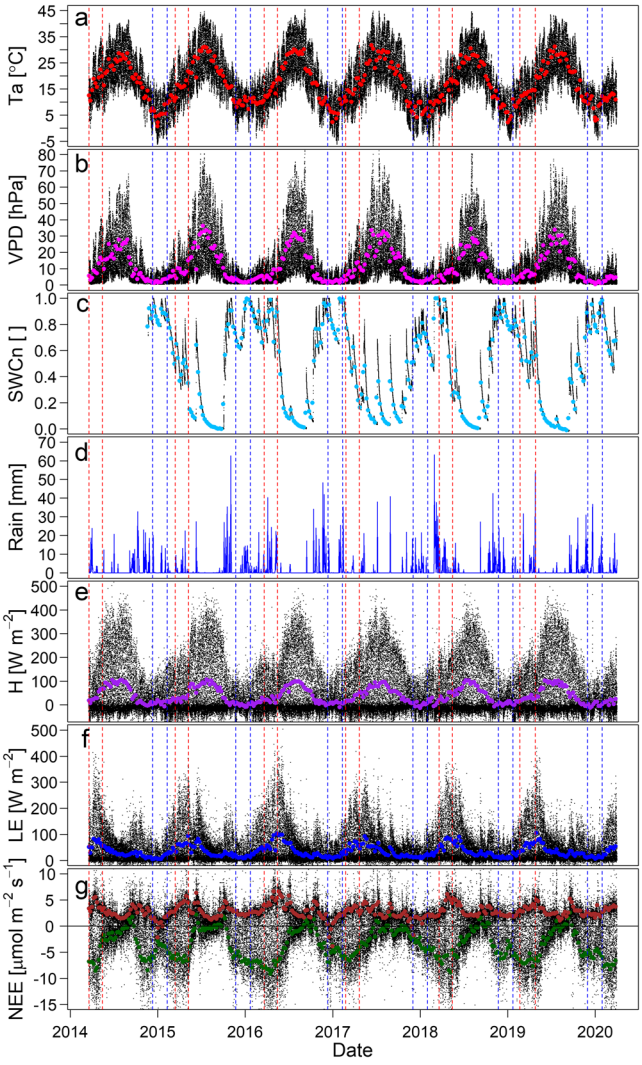

Figure 1. Flux and meteorological overview of the control plot from March 2014 to March 2020. Small black dots are half hourly data and the big colored points correspond to weekly averages. Ta is the air temperature in 2 m (a), VPD is vapor pressure deficit in 2 m (b), SWCn is the normalized soil moisture content for the top 20 cm (c), Rain are daily precipitation sums (d), H is the sensible heat flux (e), LE is the latent heat flux (f), NEE is the net ecosystem exchange of carbon dioxide (g) big green dots are daytime averages and big brown dots are night time averages. The vertical dashed lines correspond to the winter (blue) and spring period (red).

We present here, 6 years (2014–2020) of data from a large-scale N and P manipulation experiment, in which we combine eddy covariance data with satellite and plant trait data. We measured and compiled ecosystem responses of water fluxes [evapotranspiration (ET), transpiration (T), evaporation (E)], carbon fluxes [net ecosystem exchange (NEE), gross primary productivity (GPP), ecosystem respiration (Reco)], and different metrics of WUE (i.e., the carbon uptake per unit of water lost), with changes in canopy structure (leaf area index, LAI) and foliar nutrient content and isotopes, mainly during the winter and spring period.

We analyze the available data streams to evaluate if and how changing nutrient availability and stoichiometric N:P imbalance influences carbon and water fluxes, canopy structure and WUE at ecosystem scale.

2. Material and Methods

2.1. Site Description

The study site, Majadas de Tiétar (Casals et al., 2009; El-Madany et al., 2018; Perez-Priego et al., 2017), is located in the center of the Iberian Peninsula (39°56′25″N 5°46′29″W). It is a tree-grass ecosystem, a typical "*Iberic dehesa*," with 20–25 *Quercus ilex* trees ha^{-1}. The average canopy height is 8.7 ± 1.25 m, and the fractional canopy cover is 23.0 ± 5.3% (Bogdanovich et al., 2021). The *dehesa* is managed and used for extensive cattle farming with a cow density of ≤ 0.3 ha^{-1}. Precipitation and temperature were measured at the site between 2004 and 2019. The mean annual precipitation was 636 mm, ranging from 440 to 965 mm. Nearly 85% of the annual precipitation fell between October and April. The mean annual temperature was 16.7°C with a mean annual minimum temperature of −4.7°C and a mean annual maximum temperature of 41.1°C. The mean LAI of the green vegetation (LAI_{green}) changes throughout the seasons, with a mean value between 0.25 ± 0.07 m^2 m^{-2} in summer and 1.75 ± 0.25 m^2 m^{-2} at the peak of the growing season in spring, for the herbaceous layer and between 1.5 and 2.0 m^2 m^{-2} for the trees. Due to their fractional tree canopy cover, this converts to 0.3–0.4 m^2 m^{-2} for the total area. The trees have a rather constant LAI throughout the year and seasonal variability of the ecosystem LAI is driven by the phenology of the herbaceous layer (Luo et al., 2018). The growing season begins with the re-greening of the herbaceous layer after the autumn rains start, which usually is in October (Figure 1). The growing season lasts usually until the end of April to the end of May when the depletion of soil moisture, high radiation and temperatures lead to the senescence of the herbaceous layer.

The soils are characterized as Abruptic Luvisol with a sandy upper layer (Nair et al., 2019). The prevailing wind directions are west-southwest and east-northeast.

2.2. Experimental Design and Fertilization

The study-site was divided into three plots. N was added to one plot (NT), N + P to another one (NPT), and the third plot served as the unfertilized control area (CT).

The fertilizers were applied with a tractor around the eddy covariance towers. The fertilized areas were 21.5 and 16.9 ha at NPT and NT, respectively (Figure 2). Phosphorus (50 kg P ha^{-1}) in the form of triple superphosphate [$Ca(H_2PO_4)_2$] fertilizer, was applied in November 2014 at the NPT. In March 2015, NPT and

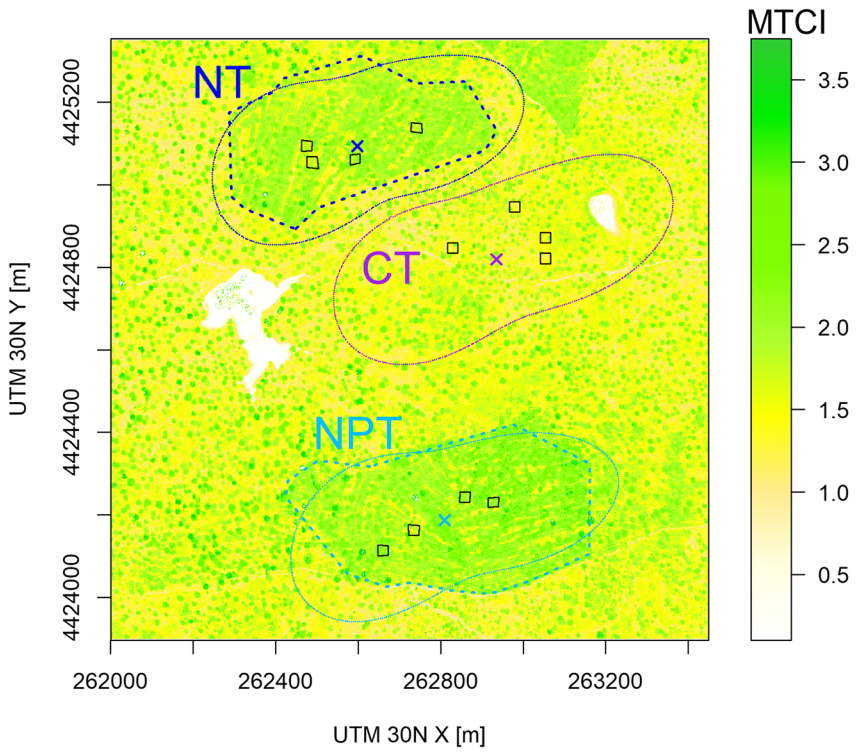

Figure 2. Post-fertilization MERIS Terrestrial Chlorophyll Index (MTCI, a vegetation index associated with the chlorophyll content of vegetation) values from hyperspectral airborne CASI images (April 23, 2015) of the study site. Tower locations are indicated with a cross in the center of the respective footprint climatology (80% isolines). The purple symbols represent the control (CT), dark blue the nitrogen (NT) and light blue the nitrogen + phosphorus (NPT) treatment. Colors represent MTCI values and indicate the degree of canopy chlorophyll concentration from yellow (low) to green (high). Green circular structures are trees. The dashed lines mark the outer limits of the fertilized areas. The green line structures within the treatments are tractor tramlines from the application of fertilizer. The white areas are water bodies.

NT received 100 kg N ha^{-1} in the form of ammonium nitrate (NH_4NO_3) and calcium ammonium nitrate ($5Ca(NO_3)_2NH_4NO_3$), respectively. Calcium ammonium nitrate was used at NT to account for the calcium included in the triple superphosphate fertilizer used at NPT. A second dose of fertilizer was applied in March 2016, 10 kg P ha^{-1} and 20 kg N ha^{-1}, using the same fertilizers as before. No further additions of nutrients were made to follow the outcome of the added nutrients and the ecosystem response in time.

2.3. Eddy Covariance Data

2.3.1. Eddy Covariance Setup

Three ecosystem eddy covariance (EC) towers are operated at the site, one in each plot. The long-term FLUXNET site Majadas de Tiétar (ES-LMa in FLUXNET, since 2003) serves as CT, and two additional towers are added for the fertilization experiment and are operated since March 2014. These EC towers are named ES-LM1 (NT) and ES-LM2 (NPT). Each tower is equipped with a R3-50 sonic anemometer (Gill Instruments Limited, Lymington, UK) to measure three-dimensional wind components and sonic temperature, and a LI-7200 infra-red gas analyzer (Licor Bioscience, Lincoln, Nebraska, USA) to measure CO_2 and H_2O mixing ratios. The measurement height is at all towers 15 m above ground.

2.3.2. Data Treatment, Gap-Filling and Partitioning

Eddy covariance data and meteorological data were collected and calculated, as described in El-Madany et al. (2018). The processing of the raw high-frequency data was conducted using EddyPro v 6.2.0 (Fratini & Mauder, 2014). Calculated CO_2 fluxes were storage corrected from seven-point profile measurements.

A friction velocity (u*) threshold [0.194 ± 0.03 ms^{-1} (CT), 0.200 ± 0.03 ms^{-1} (NT), 0.207 ± 0.02 ms^{-1} (NPT); mean ± sd] was determined for each year following Papale et al. (2006), and all data with u* values below the established threshold were removed from further analysis. The gap-filling of missing and bad quality data [QC values > 1 according to Mauder and Foken (2011)] was then performed (Reichstein et al., 2005). Subsequently, flux partitioning of NEE into GPP and Reco was conducted by applying the nighttime flux partitioning method (Reichstein et al., 2005). All post-processing was conducted using the R package REddyProc v 1.2.2 (Wutzler et al., 2018). The details of the full processing including statistics on the number of gaps for the individual fluxes are provided in the Supplementary Material and Figure S1.

2.3.3. Flux Footprint Calculations

To estimate which areas were sampled by the EC systems and to evaluate how similar these areas were the flux footprint (FP) model of Kljun et al. (2015) was used, as integrated into the Flux Footprint Prediction (FFP)-R-code version 1.4 (available at http://footprint.kljun.net/download.php). We calculated the FPs for all half-hourly (HH) periods between March 2014 and February 2020, when all input parameters (wind speed, wind direction, the standard deviation of lateral wind component, u*, Obukhov length and boundary layer height) for the model were available and friction velocity values were above the u*-threshold. The boundary layer height estimates were used from ERA5 at 0.25-degree spatial resolution (Hersbach et al., 2018) and linearly interpolated to fit the 30-min temporal resolution of the EC data. The flux footprint climatology (FFC) was subsequently calculated based on 64271 (CT), 66920 (NT), and 67862 (NPT) individual HH footprints, by integrating the flux contribution from the peak location into all directions until that is, 80% of the total contribution was reached. The 80% contribution was selected because it was the largest at which no overlap between the treatments was observed (Figure 2). The size of the FFC for the three plots were 26.0 ha (CT), 23.2 ha (NT), and 24.3 ha (NPT). At NT and NPT the fertilized areas covered 16 and 19.1 ha centered on the respective FFC.

The FFC was intersected with Landsat 7 Normalized Difference Vegetation Index (NDVI) maps (see 2.4.1) and classification maps from airborne hyperspectral measurements (see 2.4.2 and Pacheco-Labrador et al. (2017; 2020)) to calculate, for example, average NDVI values, tree canopy cover and FFC size. The medians of the distribution of tree and grass fraction from the individual HH FPs of all treatments agree within 2% with the fractional cover within the FFC. Between treatment differences of the fractional covers were below 6% (Figure S2) for the FFC as well as the medians of the HH flux footprints.

2.4. Remote Sensing Data

2.4.1. Landsat Data

The Landsat 7 NDVI at 30 m spatial resolution (Masek et al., 2006) data were obtained from Google Earth Engine Data Catalog (https://developers.google.com/earth-engine/datasets/catalog/LANDSAT_LE07_C01_T2_SR#description) and were used to characterize pre-fertilization (1999–2014) and post-fertilization (2015–2019) differences within the 80% isolines of the FFC at each tower (Figure S3). First, a subset including the outer margins of the 80% FFCs was taken from each scene. Depending on their size individual FFC included 264 to 294 30 × 30 m Landsat 7 pixels. After May 31, 2003, the Scan Line Corrector (SLC) of Landsat 7 broke, which resulted in a reduction of available pixels per scene. The data gaps form alternating wedges that increase in width from the center to the edge of a scene and change position in the different overpasses. Additionally, the following quality control scheme was used to ensure that pixels within the subsetted scenes were cloud-free and of good quality: Atmospheric opacity ≤0.1, cloud cover ≤2, pixel quality ≤66 and pixel saturation = 0. In case that more than 20% of the pixels were flagged as bad quality the whole scene was removed from the analysis. The lowest number of good quality pixels within the FFCs for an individual scene ranged between 60% and 68% of all available pixels (including data gaps due to SLC error). Average NDVI values were calculated for each treatment's FFC when the quality of the respective scene was good. Overall, 170 and 92 scenes fulfilled the quality criteria for the pre- and post-fertilization periods, respectively.

2.4.2. Airborne Spectral Measurements

Airborne hyperspectral measurements were conducted using a Compact Airborne Spectrographic Imager CASI-1500i (CASI) (Itres Research Ltd., Calgary, AB, Canada) with a spatial resolution of 1.25 m and 140 spectral bands ranging from 380 to 1,050 nm (Pacheco-Labrador et al., 2017, 2020). The CASI was on board a C-212-200 RS airplane, which was operated by the Spanish Institute for Aerospace Technology. Hyperspectral flight campaigns were conducted on May 5, 2011 (before the experiment), April 8, 2014 (during the experiment but before the fertilization), and April 23, 2015 (after the fertilization) around solar noon and using similar flight patterns. The Envisat MEdium Resolution Imaging Spectrometer (MERIS) Terrestrial Chlorophyll Index (MTCI) was calculated based on the CASI data, to have an estimate of canopy chlorophyll content in the different treatments (Dash & Curran, 2007).

$$MTCI = \frac{\rho 753.75 - \rho 708.5}{\rho 708.5 + \rho 681.25} \tag{1}$$

Here, ρ is the hemispherical-directional reflectance factor for a specific wavelength in nm. The numbers denote the wavelengths. Similarly, NDVI was calculated from the CASI data following Rouse et al. (1974).

$$NDVI = \frac{\rho_{800} - \rho_{670}}{\rho_{800} + \rho_{670}} \tag{2}$$

For details about the processing of the hyperspectral images we refer to Pacheco-Labrador et al. (2017, 2020). The number of CASI pixels within each FFC ranged, depending on its size, between 148763 – 166350. MTCI and NDVI values from pixels classified as water bodies were excluded from the analysis. Differences between distributions were then used to estimate the effect of the fertilization (Figure S4).

2.5. Ecosystem Functional Parameter

2.5.1. Metrics of Photosynthetic Capacity

The maximum net CO_2 uptake rate of the canopy at infinite global radiation (A_{max}) was calculated as part of the daytime flux partitioning (Lasslop et al., 2010) as implemented in ReddyProc v.1.2.2 and described in Wutzler et al. (2018 Chapter 2.3.2 Equations 2 and 3) using a rectangular hyperbolic light response curve (LRC, Equation 3).

$$NEE = \frac{\alpha * A_{\max} * R_g}{\alpha * R_g + A_{\max}} + \gamma \tag{3}$$

where Rg is the global radiation, α the initial slope of the LRC and γ the Lloyd and Taylor respiration model (Lloyd & Taylor, 1994). We want to emphasize, that A_{max} includes a VPD dependency based on an exponentially decreasing function at VPD values > 10 hPa).

To calculate the GPP value at light saturation that is, $R_g = 1{,}000\ W\ m^{-2}$ (GPP_{sat}), the "*light.response*" function of the "*bigleaf*" R-package (Knauer et al., 2018 Equation 29) was used as shown in Equation 4.

$$-NEE = \frac{\alpha\, R_g}{\left(1 - \left(\frac{R_g}{R_{gRef}}\right) + \left(\frac{\alpha\, R_g}{GPP_{sat}}\right)\right)} - R_{eco} \tag{4}$$

where α is the initial slope of the LRC, R_{gRef} the reference R_g of 1,000 W m^{-2}, and R_{eco} the ecosystem respiration. The parameters α and GPP_{sat} are derived using the "*nls*" function in R (R Development Core Team, 2015). GPP_{sat} was calculated for every day using a three-day moving window.

2.5.2. Water-Use Efficiency Metrics

We used the stomatal slope parameter G_1 as a physiologically significant WUE metric from the eddy covariance data (Knauer et al., 2018). It is calculated based on the stomatal model of Medlyn et al. (2017) and is inverse to the WUE.

$$G_s = G_0 + 1.6\left(1 + \frac{G_1}{\sqrt{VPD}}\right)\frac{GPP}{C_a} \quad (5)$$

G_s is the surface conductance for water vapor, G_0 is the minimum canopy conductance, G_1 is the stomatal slope parameter, VPD the vapor pressure deficit, Ca the CO_2 concentration and GPP is the gross primary productivity.

For the calculation of G_1, the R package "*bigleaf*" was used (Knauer et al., 2018). To ensure meaningful estimates of G_1, data were first filtered for the following reasons: 1) to only include measured, flux and meteorological input parameters (no gap-filled data); 2) to remove 48 h after precipitation; and to ensure that values were within the following ranges 3) global radiation (Rg) > 100 W m^{-2}; 4) GPP > 1 μmol m^{-2} s^{-1}; 5) VPD > 0.1 kPa; 6) LE and net radiation (Rn) > 0 W m^{-2}; and 7) relative humidity (rH) < 95%. After filtering, 18% (CT), 20% (NT), and 20% (NPT) of the site data remained. The difference of 2% in data availability was due to a longer data gap at the CT plot, which was caused by lightning in the summer of 2014. G_s was calculated based on the inverted Penman-Monteith equation (Knauer et al., 2018 Equation 15), where aerodynamic conductance was estimated, according to Thom et al. (1972). G_1 was then calculated for the spring of each year, individually, to compare the changes in G_1 between sites and pre- and post-fertilization. The uncertainty of G_1 was estimated by randomly resampling 10% of the data used to calculate G_1. This procedure was repeated 100 times for each spring season of each year (2014–2019).

To estimate the fertilization effect on G_1 the pre-fertilization G_1 estimate for spring 2014 was subtracted from each post-fertilization G_1 estimate for the respective spring periods (2015–2019). Thus, the differences between G_1 at the CT plot and fertilized treatment plots (NT, NPT) correspond to the fertilization effect. To compare whether different WUE metrics detected the same patterns we also calculated inherent WUE (iWUE, Beer et al., 2009) and underlying WUE (uWUE, Zhou et al., 2014) for the same time periods as G_1. The descriptions of the different WUE formulations are described in the SI.

2.5.3. Transpiration Estimates

The transpiration estimation algorithm (TEA) was used to partition measured ET into T and E (Nelson et al., 2018). TEA operates by modeling ecosystem WUE_T (as GPP/T) from GPP and ET data after controlling for E contamination in the ET signal. First, the data is filtered for periods when plants are active (i.e., GPP > 0.5 gC m^{-2} d^{-1}) and when ecosystem surfaces are probably dry to minimize the influence of abiotic evaporation. A machine learning model [random forest (Breiman, 2001)] was then trained on the WUE_{ET} (as GPP/ET) within this filtered subset using metrics derived from the eddy covariance fluxes and associated meteorological data as predictors. The trained model then predicts WUE_T at every time step using a 75% quantile prediction (Meinshausen, 2006) to further account for the effect of residual E in the training data set. The 75% quantile was chosen based on previous experiments using the model output as synthetic eddy covariance data when T was known (Nelson et al., 2018). T is then ultimately calculated as GPP/WUE_T. See Nelson (2020) for the related code and tutorials describing the use of TEA.

2.6. Vegetation Data

Every year, the herbaceous layer was sampled in spring to measure biomass, green LAI and to analyze nutrient content. At each sampling date (Table 1), the aboveground biomass was harvested in multiple 25 × 25 cm squares of the herbaceous layer within the 25 × 25 m plots in each FFC (Figure 2). A subsample of the total biomass was selected and green and senescent fractions were separated by hand in the laboratory. The green and senesced fractions were weighted, scanned, dried and weighted again. The LAI_{green} was then calculated as

Table 1
Number of Samples for Nutrient Analysis for the Herbaceous Layer per Treatment and Sample Date

	2014-04-08	2015-04-23	2015-05-28	2015-07-08	2016-05-03	2016-05-20	2017-05-01	2017-05-18	2018-07-17
CT	24	24	8	24	24	10	12	25	6
NT	7	8	8	8	8	4	11	12	4
NPT	6	8	8	8	8	2	12	12	8

$$LAI_{green} = \frac{\frac{W_{DT} * W_{DSG}}{W_{DS}} * LAI_{greenSub}}{W_{DSG} * A_T} \quad (6)$$

With W_{DT} the dry weight of the total sample, W_{DSG} the the dry weight of the green fraction of the subsample, W_{DS} the dry weight of the subsample, $LAI_{greenSub}$ the leaf area of the green fraction of the subsample and A_T the area of the sample plot. Samples were oven-dried at 60°C for 48 h. Plant material was ground using a ball mill (Co. Resch) at a frequency of 20 Hz for less than 4 min. Subsequently, the material was stored for further chemical analysis.

N concentration (mg/g) was analyzed by the dry combustion method (Vario EL; Elemantar GmbH, Hanau, Germany) using 25 mg of the ground sample material.

P concentrations were analyzed using an inductive coupled plasma optical emission spectrometer (ICP OES, Optima 3300, Perkin Elmer). First 0.1 g of the dried and ground plant material was weighed and 3 ml of HNO_3 were added. The sample was then heated for 20 min with 1,000 W and then cooled down for 10 min. Afterward, the sample was filtered and diluted with deionized water to get a 50 ml sample. The prepared sample was then analyzed in the ICP OES.

Isotopic signatures are based on the determination of the carbon isotopic composition of dried grass and tree foliar samples. They were analyzed with a DeltaPlus isotope ratio mass spectrometer (Thermo Fisher, Bremen, Germany) coupled via a ConFlowIII open-split to an elemental analyzer (Carlo Erba 1100 CE analyzer; Thermo Fisher Scientific, Rodano, Italy). The measurement protocol is based on Werner et al. (1999; 2001) and Brooks et al. (2003). Carbon isotope signatures of tree and grass samples ($\delta^{13}C$) were calculated using Equation 7.

$$\delta^{13}C = \frac{{}^{13}R_{sample} - {}^{13}R_{standard}}{{}^{13}R_{standard}} \quad (7)$$

Here ^{13}Rsample is the $^{13}C/^{12}C$ ratio of the respective sample, and ^{13}RStandard is the $^{13}C/^{12}C$ ratio of the standard. All values are in per mil (‰) by multiplying the $\delta^{13}C$ values by a factor of 1,000 (Brand, 2013; Coplen, 2011). The $\delta^{13}C$ values are based on the δ^{13}CIAEA-603 – LSVEC scale. Samples were analyzed against a calibrated in-house-standard (Acetanilide: −30.06 ± 0.05‰). Additionally, a quality control standard (Caffeine: −40.46‰) was interspersed between samples. The precision of the sequences was smaller or equal to 0.1‰.

Table 2
Number of Samples for Stable Carbon Isotope Signature and Nutrient Analysis for the Quercus Ilex Trees per Treatment and Sample Time

	2013-11-01	2014-03-01	2015-12-01	2016-12-12	2017-12-01
CT	24	8	7	7	7
NT	24	8	6	6	6
NPT	24	8	6	6	6

The leaf samples of the Quercus ilex trees were analyzed in the same way as the samples of the herbaceous layer. The only difference were the sampling dates (Table 2). For the Quercus ilex, the leaf sampling was done during the winter period when the foliar nutrient concentrations are more stable. Sampling times and numbers are shown in Table 2. For nutrient analysis branches from the upper third of the crown (both North and South orientations) were detached and 100 leaves per tree were sampled. Between 6 and 8 trees (except for 2013 when 24 trees were sampled) were sampled per treatment (Table 2).

2.7. Statistical Analysis

2.7.1. Estimation of Fertilization Effects and Uncertainties

To quantify the changes in carbon and water fluxes after the fertilization the pre-fertilization differences and post-fertilization differences between the treatments were assessed. We identified two sources of uncertainty for this comparison that relate to (1) within-FFC heterogeneity and (2) differences in seasonality and interannual variability (IAV) between treatments (Figure S5). These independent sources of differences and uncertainty were considered by following the subsequent steps:

1) Within-FFC heterogeneity was accounted for by calculating between-treatment flux differences at a half-hourly temporal scale. The variability in meteorological conditions and wind direction modifies the location and size of each footprint. The vegetation properties of the different footprints vary according to microtopography, tree density, and species composition of the herbaceous layer within each footprint. Since these factors are not spatially correlated between FFCs, this variability must be accounted for when assessing the overall signals of the footprint climatologies. Before fertilization, flux differences carry information about pre-fertilization differences, spatial variability, and flux uncertainties (El-Madany et al., 2018). After fertilization, the effect of nutrients could be reflected in both the average difference between fluxes and the variability within the FFCs.

To characterize the differences between treatments and the uncertainty that the intra-FFC variability causes in the determination of such differences, the half-hourly fluxes in the unfertilized, or CT were subtracted from those of the fertilized treatments (NT and NPT). For half-hourly (HH) differences for a flux (F) between NT and CT, this would be:

$$\Delta F_i = NT_i - CT_i \tag{8}$$

where Δ indicates the difference between a treatment and the control, F is any flux of interest (e.g., GPP or ET), and i stands for any individual half-hour. Due to the proximity of the treatments, the meteorological conditions (e.g., atmospheric pressure, precipitation, shortwave- and longwave incoming radiation, wind speed, wind direction, air temperature) are virtually identical for all treatments (data not shown). Therefore, the distribution of ΔF_i within a particular time window (e.g., spring$f(\Delta F_i)$) holds information about the mean ($\mu_{\Delta F_i}$) flux differences between the control and fertilized treatments and the variability within the FFCs. The associated uncertainty ($\bar{\sigma}$) is determined as the effective standard error ($\bar{\sigma}_{\Delta F_i}$):

$$\bar{\sigma}_{\Delta F_i} = \frac{\sigma_{\Delta F_i}}{\sqrt{n_{eff}}} \tag{9}$$

with $\sigma_{\Delta F_i}$ being the standard deviation of $f\left(\Delta F_i\right)$ and n_{eff} the effective number of observations.

n_{eff} accounts for the autocorrelation of the time series and was estimated using the first coefficients of the empirical autocorrelation function, as described by Wutzler et al. (2019). The empirical autocorrelation function was estimated using continuous and, thus, gap-filled time series. The gap-filled time series were smoother than the time series that excluded gaps; thus, both the autocorrelation and the resulting uncertainty were probably conservatively overestimated.

2) In our study, the fluxes measured in 2014 served as the pre-fertilization reference where all treatments were measured in parallel and, thus, allowed us to estimate the between-treatment differences for each season. The use of only 1 year as the baseline to determine the treatment effect might be hampered by the fact that flux magnitude varies between different years and seasons according to meteorological conditions, and proper characterization of the differences in the interannual variability of fluxes before fertilization is not possible.

To overcome such a limitation, we used the Landsat NDVI time series for the period 1999–2019 calculated for each FFC. Optical remote sensing is sensitive to vegetation, structural, and biochemical properties, including LAI and chlorophyll content (Baret & Buis, 2008; Homolová et al., 2013), and is, therefore, suitable to quantify the differences and variability of vegetation properties in different FFCs. We estimated the linear relationship from NDVI between the control and fertilized plots. The long-term NDVI relationship

Table 3
Dates and Duration of Each Spring and Winter Season Used for the Analysis Separated by Year

Year	Spring	Winter
2014	Mar 20–May 15	Dec 11–Feb 10
2015	Mar 15–May 10	Nov 22–Jan 22
2016	Mar 20–May 15	Dec 11–Feb 10
2017	Feb 24–Apr 21	Dec 01–Jan 31
Duration	56 days	61 days

between the FFC of the treatments was considered as the average long-term pre-fertilization relationship between the treatments. Since NDVI values within the FFC are expected to have similar variance and errors, reduced major axis regression was performed using the "*lmodel2*" package version 1.7–3 (Legendre, 2018; Legendre & Legendre, 1998) in R (R Development Core Team, 2015).

Because NDVI is a good proxy of greenness and relates to ecosystem productivity, the relative deviation between the 2014 NDVI values and the long-term linear regression, can be interpreted as the relative pre-fertilization uncertainty originating from using only 2014 as a reference year instead of using a long-term average. The resulting uncertainties were 4.6% and 3.3% for CT/NT and CT/NPT, respectively. Using the assumption that the relative error of a flux F was similar to the relative error of NDVI, the corresponding pre-fertilization uncertainty for NT was calculated as:

$$\bar{\sigma}_{\Delta F_i Pre} = \mu_{\Delta F_i Pre} * 0.046 \quad (10)$$

As the relative pre-fertilization uncertainty is derived from a linear relationship, it depends on the value of the mean differences (i.e., $\mu_{\Delta F_i Pre}$). Following Equation 8–10 and assuming the error components to be independent, the total fertilization effect (FE) of F in a particular post-fertilization year and season and its associated uncertainty (FE_{unc}) is:

$$FE \pm FE_{unc} = \mu_{\Delta F_i} - \mu_{\Delta F_i Pre} \pm \sqrt{\bar{\sigma}_{\Delta F_i}{}^2 + \bar{\sigma}_{\Delta F_i Pre}{}^2} \quad (11)$$

The same procedure was followed for all spring and winter periods, years, and flux variables (Figure 4, S5). The individual seasons were selected to cover their key features. The spring periods last for 56 days each and capture the peak of the growing season. The winter periods last for 61 days and cover the lowest seasonal temperatures. Table 3 shows the exact starting and ending dates for each season used in the analysis and in Figure 1 the respective meteorological conditions and flux magnitudes can be seen. Due to the variability in meteorological conditions the starting and end dates of each season change from year to year but they always have the same length.

2.7.2. Seasonal and Annual Sums

To estimate the impact of fertilization on carbon and water fluxes and the WUE of the ecosystem, we calculated annual and seasonal cumulated sums (Table 4). The differences between the fertilized and control treatments were then used to calculate the fertilization effect on the annual and seasonal sums. We emphasize that differences between the fertilization effects from the high-quality half-hourly data and the gap-filled cumulated sums are expected. The main reason is the larger fraction of good quality EC data during daytime hours compared to nighttime data.

2.8. Functional Relations and Regression Analyses

To characterize the changes of functional properties due to fertilization, we analyzed the relationships between LAI and LAI * [N] with A_{max}, GPP_{sat}, and G_s for each treatment, individually. The goodness of fit allows us to evaluate whether leaf [N] partially explains the respective relationships or not. LAI and leaf [N] were based on spatial sampling within the FFC of the treatments, and the values A_{max} and GPP_{sat} were time averages for periods of ±7 days around the sampling date as individual values were only calculated every second day. The G_s values were averaged for the same period but were based on midday values between 12:00 and 14:00 UTC. Linear, nonlinear, and segmented regressions were fitted to the data.

Linear and nonlinear least squares regressions were performed in R using the "lm" and "nls" functions (R Development Core Team, 2015), respectively. The nonlinear regressions used the following formula to

Journal of Geophysical Research: Biogeosciences 10.1029/2020JG006005

Table 4
Average Seasonal (Spring, Winter) and Annual Carbon (C) and Water (H_2O) Fluxes for the Control (CT), Nitrogen (NT), and Nitrogen + Phosphorus Treatments (NPT)

Season	Spring			Winter			Annual		
Variable	NEE	GPP	Reco	NEE	GPP	Reco	NEE	GPP	Reco
Unit					$gC\ m^{-2} \pm unc$				
C-Flux CT	−46.8 ± 6.0	309.0 ± 7.3	262.2 ± 8.5	−12.4 ± 13.6	141.4 ± 15.7	129.0 ± 11.3	75.0 ± 20.6	1,073.2 ± 23.5	1,148.2 ± 25.8
C-Flux NT	−73.5 ± 6.6	348.4 ± 7.5	274.9 ± 10.3	−22.5 ± 7.6	160.4 ± 5.6	137.9 ± 5.9	−7.0 ± 18.5	1,204.8 ± 29.5	1,197.8 ± 33.1
C-Flux NPT	−69.4 ± 6.3	352.6 ± 8.0	283.2 ± 8.9	−26.1 ± 12.0	161.0 ± 19.5	134.9 ± 16.2	0.4 ± 22.6	1,216.4 ± 41.3	1,216.7 ± 29.2
ΔC-Flux NT	−26.7 ± 6.8 (−57%)	39.4 ± 7.0 (13%)	12.7 ± 11.0 (5%)	−10.1 ± 19.9 (82%)	19.0 ± 16.3 (13%)	8.9 ± 15.8 (7%)	−81.9 ± 25.9 (−109%)	131.6 ± 31.2 (12%)	49.6 ± 45.4 (4%)
ΔC-Flux NPT	−22.6 ± 12.7 (−48%)	43.6 ± 18.7 (14%)	21.0 ± 19.0 (8%)	−13.7 ± 23.1 (−110%)	19.6 ± 18.9 (14%)	5.9 ± 14.2 (5%)	−74.6 ± 19.9 (−100%)	143.2 ± 46.7 (13%)	68.5 ± 54.4 (6%)
Variable	ET	T	E	ET	T	E	ET	T	E
Unit					$kgH_2O\ m^{-2} \pm unc$				
H_2O-Flux CT	122.7 ± 2.2	92.9	28.7	29.4 ± 1.1	14.2	14.8	470.2 ± 4.8	307.3	156.1
H_2O-Flux NT	130.3 ± 2.3	105.3	25.0	31.1 ± 1.1	18.9	12.2	518.7 ± 5.0	364.8	151.0
H_2O-Flux NPT	121.0 ± 2.2	97.3	23.7	27.6 ± 1.2	17.1	10.5	463.4 ± 4.6	328.9	132.3
ΔH_2O -Flux NT	7.6 ± 8.7 (6%)	12.4 ± 6.3 (13%)	−3.7 ± 4.9 (−13%)	1.7 ± 2.8 (6%)	4.7 ± 2.1 (33%)	−2.6 ± 4.7 (−18%)	48.6 ± 28.3 (10%)	57.5 ± 30.0 (19%)	−5.1 ± 11.3 (−3%)
ΔH_2O -Flux NPT	−1.8 ± 5.1 (−1%)	4.4 ± 3.8 (5%)	−5.0 ± 2.8 (−18%)	−1.7 ± 3.6 (−6%)	2.9 ± 1.3 (21%)	−4.3 ± 3.7 (−29%)	−6.7 ± 12.2 (−1%)	21.6 ± 16.9 (7%)	−24.2 ± 8.7 (−16%)

The averages are based on the 5 years of the post-fertilization period between March 2015 and February 2020. The displayed fluxes are net ecosystem exchange (NEE), gross primary productivity (GPP), ecosystem respiration (Reco), evapotranspiration (ET), transpiration (T), and evaporation (E) including their respective uncertainties (± unc). All carbon fluxes include the mean uncertainty based on u* filtering and the uncertainty of marginal distribution sampling for NEE. For ET, the flux uncertainty was estimated based on marginal distribution sampling. All uncertainties were calculated for each season and year and then propagated based on standard error propagation. The fertilization effects (Δ) were calculated as the difference between the fertilized and control treatment including the respective standard deviations (± sd) to show the year to year variability of the fertilization effects. Additionally, the relative change compared to the control is given as percent.

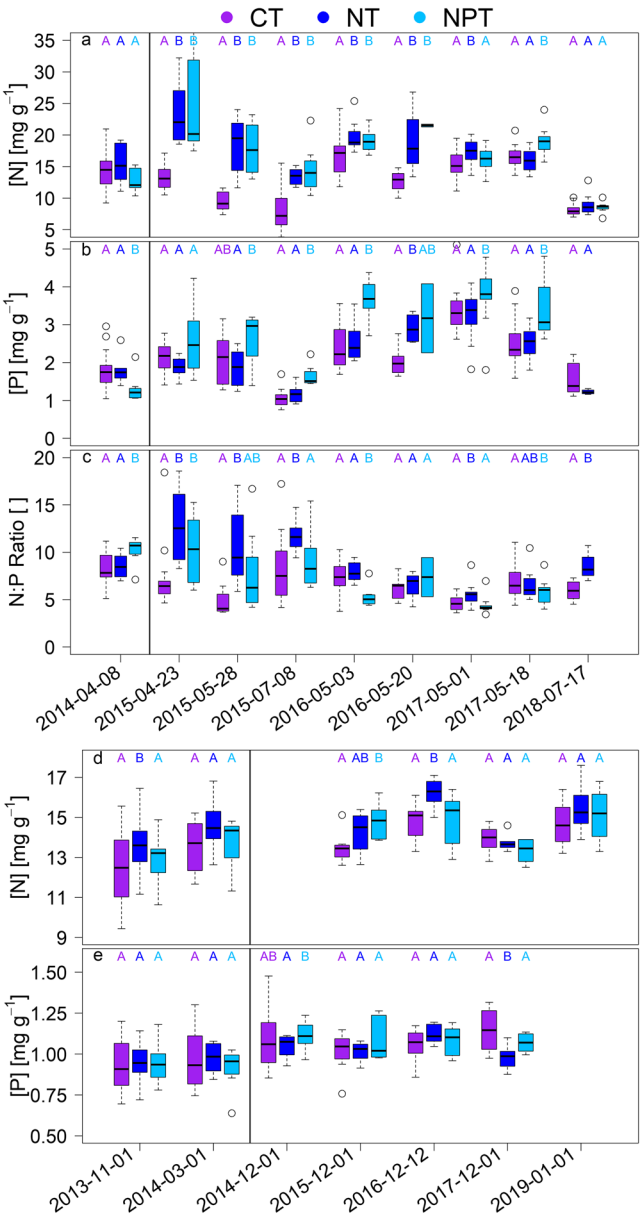

Figure 3. Nitrogen (N) and phosphorous (P) concentration for the herbaceous layer (a), (b) and tree leaves (d), (e) as well as the N:P ratios (c) for the herbaceous layer. Samples are from within the footprint areas of the control (CT, purple), nitrogen (NT, blue), and nitrogen + phosphorus treatments (NPT, light blue). The black vertical line separates the pre- and post-fertilization periods. Letters above boxplots indicate significant differences between treatments at the $p < 0.05$ level based on the two-sided Wilcoxon test.

characterize the saturating behavior of a relationship in which the parameters a, b, and c were optimized to minimize the residual sum of squares (RSS) between model and observations:

$$y = \frac{a * x}{b + x} + c \tag{12}$$

Here, y is the property of interest (e.g., GPP_{sat}), and x is either LAI or LAI * [N]. The starting values for a, b, and c were the same for all treatments (i.e., LAI * [N] vs. GPP_{sat}) in the CT, NT, and NPT plots.

In addition to the nonlinear regressions, segmented regressions were performed using the "segmented" package (Muggeo, 2003, 2017) in R to estimate the breakpoint between the increase and plateau of the nonlinear relationship. No prior value was provided to the breakpoint estimation algorithm.

When comparing the means of two or more distributions a two-sample t-test was used. The "t.test" function in R (R Development Core Team, 2015) was used. Each distribution was tested against the others and the significant differences between means were encoded in letters to show which distributions means were significantly different from each other.

Analysis of Covariance (ANCOVA) was used to evaluate the treatment effect on changes in the linear relationship between variables. The "aov" function in R was used.

3. Results

3.1. Leaf Level Nutrients

The increase in [N] in the herbaceous layer of both fertilized treatments, NT and NPT, was most significant in the first 2 years following fertilization (2015 and 2016). In 2017, it was higher for only a few sampling periods (Figure 3). The differences in [N] between the fertilized and control treatments became smaller from 2015 to 2019.

[P] increased significantly after fertilization for all years in the NPT plot, except during the first sample in 2015. While both nutrients were taken up by the herbaceous vegetation, the resulting increased [N] reduced faster than [P]. The comparison of N:P ratios between CT, NT, and NPT showed that fertilization modified the nutrient stoichiometry of the herbaceous vegetation as expected, with a higher average N:P ratio (stoichiometric imbalance) in the NT plot (9.3 ± 2.5; mean ± s.d.) than in the CT (7.3 ± 0.8) and NPT plots (7.5 ± 2.4) (Figure 3). In contrast, the trees did not consistently vary in leaf nutrient content during the post-fertilization period (Figure 3).

3.2. Carbon Fluxes

The impact of fertilization on carbon fluxes was largest for the spring and winter periods of 2015 and 2016 (Table 4 and Figure 4). GPP generally increased, while Reco increased much less or even reduced, which caused NEE to become more negative. For the spring periods from 2015 to 2019, the average HH daytime ΔNEE was more negative in the fertilized treatments (−0.0156 ± 0.0076 gC m^{-2} (mean ± s.d.) at NT and −0.0161 ± 0.0077 gC m^{-2} at NPT). This resulted in 57% and 48% more negative cumulated spring NEE in the NT and NPT, compared

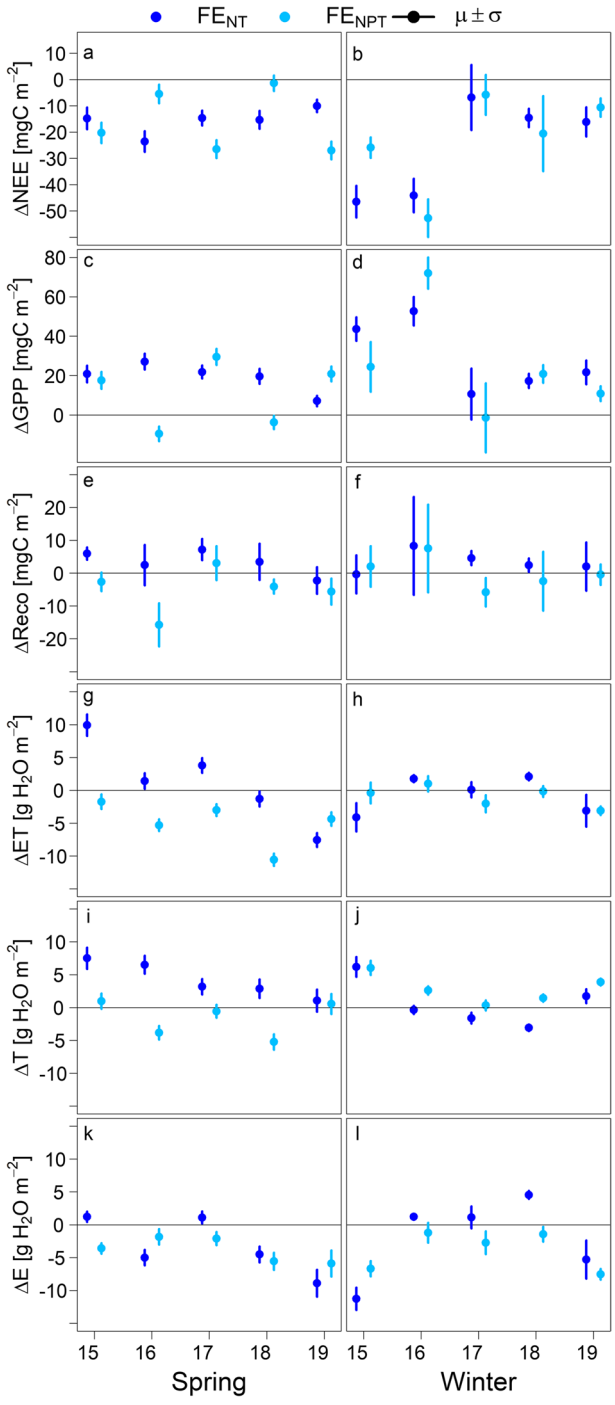

Figure 4. Mean fertilization effects (FE) for spring (left column) and winter (right column) periods from 2015 to 2019 (abbreviated as 15 to 19 on the *x*-axis) in the plots fertilized with nitrogen (NT, dark blue) and nitrogen + phosphorus (NPT, light blue), including the associated uncertainties (vertical bars). Shown are fertilization effects for net ecosystem exchange (NEE, (a), (b)), gross primary productivity (GPP, (c)), (d)), ecosystem respiration (Reco, (e), (f)), evapotranspiration (ET, (g), (h)), transpiration (T, (i), (j)), and evaporation (E, k, l).

to CT (-46.8 ± 6.0 gC m^{-2}; Table 4). Spring ΔGPP was higher in the NPT plot, $+43.6 \pm 18.7$ gC m^{-2} (14%) and $+39.4 \pm 7.0$ gC m^{-2} (13%) in the NT, while ΔReco was $+12.7 \pm 11.0$ gC m^{-2} (5%) and $+21.0 \pm 19.7$ gC m^{-2} (8%) relative to the CT (Table 4).

During winter periods, large changes in carbon fluxes were observed in the fertilized treatments. Particularly, during the first 2 years following fertilization (2015–2016, Figure 4), the average HH ΔNEE was more negative than in any other seasons or years (-0.0453 ± 0.0085 and -0.0393 ± 0.0082 gC m^{-2} at NT and NPT). The increased uptake was a result of high ΔGPP ($+0.0481 \pm 0.0094$ (NT) and $+0.0482 \pm 0.0149$ (NPT) gC m^{-2}) relative to small positive ΔReco ($+0.0039 \pm 0.016$ (NT) and $+0.0048 \pm 0.0147$ (NPT) gC m^{-2}) in both treatments.

The average cumulated winter NEE became 82% (NT) and 110% (NPT) more negative in the fertilized treatments compared to the CT (-12.4 ± 13.6 gC m^{-2}). Again, this increase in carbon uptake was driven by a substantial increase in GPP in both fertilized treatments (i.e., ΔGPP $+19.0 \pm 16.3$ gC m^{-2} (13%) in the NT and $+19.6 \pm 18.9$ gC m^{-2} (14%) in the NPT) compared to the increase in Reco.

When comparing drier (2015, 2017, 2019) and wetter (2016, 2018) spring periods, the fertilization effects vary in their strength and between treatments. The fertilization effects in dry and wet spring periods (Figure S6) were in opposite directions in the NT and NPT plots and point toward stronger carbon uptake in the NPT during drier conditions and in the NT during wetter conditions.

At the annual scale, ΔGPP was positive in the fertilized treatments $+131.6 \pm 31.2$ gC m^{-2} (12%) in the NT and $+143.2 \pm 46.7$ gC m^{-2} (13%) in the NPT, but ΔReco was less high $+49.6 \pm 45.4$ gC m^{-2} (NT) and $+68.5 \pm 54.4$ gC m^{-2} (NPT), respectively. As a result, the annual NEE changed from an average carbon source in the CT ($+75.0 \pm 20.6$ gC m^{-2}) to carbon-neutral in the NT (-7.0 ± 18.5 gC m^{-2}) and NPT ($+0.4 \pm 22.6$ gC m^{-2}) plots.

3.3. Water Fluxes

ET was highest during the spring and lowest during winter with cumulated values at CT of 122.7 ± 2.2 kgH_2O m^{-2} and 29.4 ± 1.1 kgH_2O m^{-2}, respectively. The fertilization effects on water fluxes differed between the NT and NPT. While changes in ΔET at NPT during spring and winter were on average negative, they were positive in the NT (Table 4, Figure 4). During spring and winter, the cumulated seasonal sums of T increased for both fertilized treatments, and they decreased for E. ΔT was highest in the NT ($+12.4 \pm 6.3$ kgH_2O m^{-2}; 13%) while in the NPT, it was only $+4.4 \pm 3.8$ kgH_2O m^{-2} (5%). In addition, E was substantially reduced in the NPT plot compared to the NT plot, with an overall decrease in ET in the NPT plot (Table 4).

At the annual scale, ΔET was $+48.6 \pm 28.3$ kgH_2O m^{-2} (10%) in the NT and -6.7 ± 12.2 kgH_2O m^{-2} (-1%) in the NPT. The positive ΔET in the NT was driven by the ΔT [$+57.5 \pm 30.0$ kgH_2O m^{-2} (19%)], whereas the ΔT in the NPT [$+21.6 \pm 16.9$ kgH_2O m^{-2} (7%)] was compensated by the negative ΔE [-24.2 ± 8.7 kgH_2O m^{-2} (-16%)].

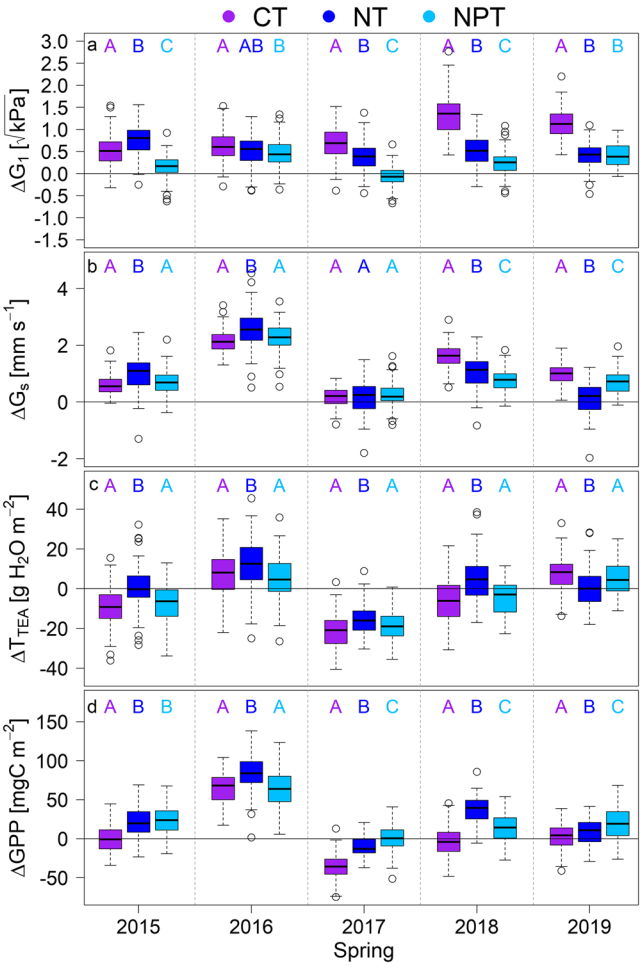

Figure 5. Between-tower differences for water-use efficiency-related parameters for the spring periods from 2015 to 2019. Boxplots for each treatment [control (CT, purple), nitrogen (NT, dark blue), and nitrogen + phosphorus treatments (NPT, light blue)] and year are the differences between the respective post-fertilization years (2015–2019) and the pre-fertilization period of 2014. The panels display the stomatal slope parameter (G_1, (a)), surface conductance (G_s, (b)), canopy transpiration based on the TEA algorithm (c), and gross primary productivity (GPP, (d)). Letters above the boxplots indicate significant differences in the means based on two-sample t-tests at the $p < 0.01$ level.

3.4. Water-Use Efficiency

Changes in carbon and water fluxes due to fertilization display increased uptake of carbon during the growing season for both treatments and a reduction in ET in the NPT in spring, while ET and T increased in the NT for the same period (Table 4). A comparison across three measures of WUE (G_1, IWUE, and uWUE) showed that they all follow the same main patterns as a result of fertilization (Figure S7). Changes in G_1, as well as G_s, T, and GPP during the post-fertilization spring periods, are reported in Figure 5. Overall, strong interannual variability with consistent treatment effects was observed.

On average, NPT had the lowest G_1 values, which means it had the highest WUE, followed by NT. Both fertilized treatments showed increased G_s and T compared to the CT. However, for both, G_s and T values of the NPT were significantly lower in most springs compared to the NT ($p < 0.01$; Figure 5). As seen in Table 4 there was less evapotranspiration and transpiration in the NPT relative to the NT plot. The values of GPP were always (except for NPT in Spring 2016) significantly higher in the NT and NPT plots ($p < 0.01$) than in the CT plot (Figure 5). Overall, the increase in WUE of the fertilized treatments, compared to the CT, was driven by the increase in GPP due to the fertilization. However, the loss of water shown by T mediated the magnitude and differences between the NT and NPT. The different behavior of GPP and G_s between the fertilized treatments resulted in different WUEs. In addition, in three out of five and four out of five post-fertilization years, G_s and T were significantly ($p < 0.01$) lower in the NPT than in the NT, respectively, indicating a better water-saving strategy in the NPT plot.

The $\delta^{13}C$ isotopic signatures from the plant samples of the herbaceous layer show similar patterns as the eddy covariance based WUE estimates. While we did not find significant differences between the treatments in the control year (2014), we observed significantly higher $\delta^{13}C$ values of the herbaceous layer in the NPT ($p < 0.05$; Figure 6). In contrast, the isotopic signatures of the herbaceous layer in the NT plot were significantly higher in the first year than in the CT plot and, thus, underline the more substantial increase in WUE in the NPT compared to the NT plot.

The $\delta^{13}C$ values agree with the average post-fertilization WUE_T estimates. WUE_T spring values were 3.327 (CT), 3.307 (NT), and 3.624 $gCkgH_2O^{-1}$ (NPT) and show the highest WUE in the NPT and similar values for the NT and CT plots.

3.5. Functional Relationships

Strong linear relationships between LAI_{green} and A_{max} [$R^2 = 0.80$ (CT), 0.93 (NT), 0.92 (NPT)] across all treatments were observed (Figure 7a). The offsets in the linear fits ranged between 10.9 and 14.3 μmol m^{-2} s^{-1}. Also, both fertilized treatments showed higher A_{max} values than the CT after fertilization.

GPP_{sat} values collapsed into a small range between 5 and 7 μmol m^{-2} s^{-1} for the sampling points of July when LAI_{green} values across treatments were below 0.5 m^2 m^{-2} and water stress was high (Figures 7b and 1). The fit of LAI_{green} and GPP_{sat} was not linear and GPP_{sat} flattened at higher LAI_{green} values (Figure 7b). The change point of the segmented regression analysis showed that the plateau started at a LAI_{green} of about 1.8 ± 0.15 m^2 m^{-2}. Similar to A_{max}, GPP_{sat} values in the CT were lowest, showing a lower photosynthetic capacity in the CT compared to the fertilized treatments.

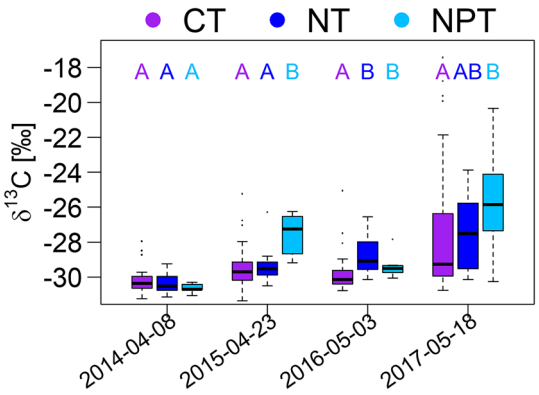

Figure 6. Isotopic signature of $\delta^{13}C$ for the herbaceous layer during the spring periods between 2014 and 2017. Boxplots display the distribution for all samples within each treatment, namely, the control (CT, purple), nitrogen (NT, blue), and nitrogen + phosphorus treatments (NPT, light blue). Letters above the boxplots indicate significant differences in the medians based on one-sided Wilcoxon tests at the $p < 0.05$ level.

The G_s were nonlinearly related to LAI_{green} similar to GPP_{sat}, and the treatments reached their plateau around 6 mm s^{-1} (Figure 7c). The highest values of G_s were detected in the NT, while NPT and CT had lower and more similar values. The largest differences between NT and the other fitted curves were detected for LAI_{green} values below 1.1 m^2 m^{-2}. The G_s values converged with increasing LAI_{green}, especially for values after the change point of the segmented regression.

When analyzing the functional relationships above with LAI_{green} * [N] the R^2 values for LAI_{green} and A_{max} increased [0.80–0.91 (CT), 0.93–0.96 (NT)] or remained similar [0.92–0.91 (NPT)] and the RSS of the LAI_{green} and GPP_{sat} reduced [11.6–7.0 μmol m^{-2} s^{-1} (CT), 6.9–3.5 μmol m^{-2} s^{-1} (NT), 2.2–2.0 μmol m^{-2} s^{-1} (NPT)]. For the relationship LAI_{green} with G_s at CT the RSS reduced, but it increased for NT and NPT.

Based on linear relationships between G_s and GPP_{sat}, the fertilized treatments have higher GPP_{sat} for the same G_s values that is, a significant difference in offset but no significant difference in slope. On the other hand, for the same increase in GPP_{sat}, the increase in G_s is highest in the NT plot but not significantly different from the NPT and CT plots (Figure S8 $p < 0.05$).

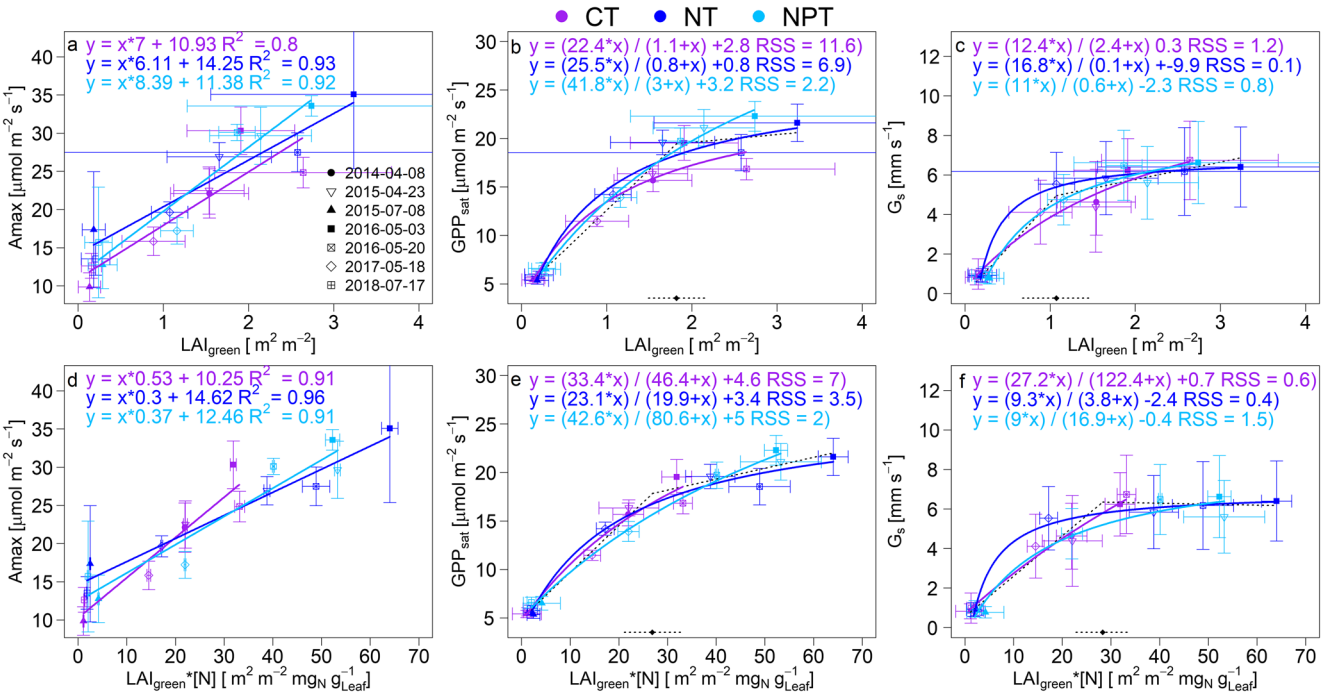

Figure 7. Functional relationships between maximum net carbon uptake (A_{max}), photosynthetic capacity (GPP_{sat}), and surface conductance (G_s) with green leaf area index (LAI_{green}, top row) and green leaf area index * nitrogen concentration (LAI_{green} * [N], bottom row) of the herbaceous layer for the control (CT, purple), nitrogen (NT, blue), and nitrogen + phosphorus treatments (NPT, light blue). All figures include the respective regression formulas and fits (solid lines). In addition, the nonlinear fits contain a segmented regression (dashed black line) with the respective breakpoint of the two linear fits and its uncertainty (black dot with dashed line at the bottom). Horizontal error bars display the standard deviation from the LAI spatial sampling, and vertical error bars display the temporal variability of A_{max}, GPP_{sat}, and midday G_s for ±7 days around the sampling day. For the nonlinear fits, the residual sum of squares (RSS) was used to show the goodness of fit.

4. Discussion

We will discuss the impacts of nutrient availability and stoichiometric imbalance on carbon and water fluxes, ecosystem-scale WUE, functional relationships, canopy structure, and nutrient content of the vegetation.

The observed changes in leaf nutrients within the herbaceous layer, but not in tree leaves, suggest that the ecosystem response to the fertilization was driven by the herbaceous layer rather than by the trees. The higher response of the herbaceous layer could be related to the common competition between trees and grasses for resources in savanna ecosystems (Riginos, 2009; Rivest et al., 2011; Sankaran et al., 2004; Scholes & Archer, 1997). The marked differences in root system profiles between the herbaceous layer and trees in the study system (Rolo & Moreno, 2012) would have allowed a higher uptake of nutrients by herbaceous species in the uppermost soil layers and hampered any response in trees. This agrees with the findings of Scalon et al. (2017), who analyzed the leaf nutrient concentrations of woody species in a Brazilian savanna in a long-term nutrient manipulation experiment and found no influence of N and P additions to the leaf nutrient concentrations. In contrast, a nutrient manipulation experiment conducted in the Harvard experimental forest for 15 years showed a constant increase in leaf nutrient content for oak and pine trees (Magill et al., 2004). The absence of increased leaf nutrients in the trees with simultaneously increased leaf nutrients of the herbaceous layer allows us to suggest that the ecosystem response to fertilization was driven by the herbaceous layer rather than by the trees. With only leaf data available, we cannot rule out that the trees have responded to the higher N availability different than increased leaf N (e.g., by increased LAI or storing N in other organs).

The strong response in carbon uptake during the first two winters following fertilization (Figure 4) could be a result of the strong mobility of N within the ecosystem. This was emphasized by the reduction of [N] during the experiment. Also, the highest N availability in the soil is expected to occur during the fall with the re-wetting of the soil after the summer drought (Joffre, 1990; Morris et al., 2019). This increased N availability then caused a faster development of the vegetation biomass (Luo et al., 2020) and higher gross and net carbon uptake rates. At the same time, the high mobility of N, due to the strong precipitation in the fall, likely leads to strong uptake via the re-greening vegetation and strong leaching of N into deeper soil layers where the herbaceous vegetation cannot access it anymore, but trees potentially could. This might lead to a continuous decrease in leaf [N] in the herbaceous layer and the strong fertilization effect being restricted to the first two winter periods. In contrast, P, which is less mobile, stayed in the system in the NPT plot and led to persistently high levels of P in the herbaceous layer at NPT.

The increased N availability can alter N:P stoichiometry in plants and result in P limitation (Du et al., 2020; Li et al., 2016; Peñuelas et al., 2013). Under these conditions, plants try to increase their P uptake (Güsewell, 2004). In a recent review, Oldroyd and Leyser (2020) describe how plants sense P availability and how they react to conditions of P limitation. The main root adaptations are increased lateral growth and elongated root hairs to more efficiently extract P, which has the highest availability in the topsoil. Nair et al. (2019) analyzed root biomass and root length density in the CT, NT, and NPT plots and found increased root biomass but no increase in root length in the NT plot; while in the NPT plot, the root mass did not increase, but the root length density did, which is in agreement with the findings of Oldroyd and Leyser (2020).

Plants increase transpiration to better extract nutrients, especially P, from the soil (Cernusak et al., 2011; Cramer et al., 2008; Huang et al., 2017; Kröbel et al., 2012; Pang et al., 2018; Rose et al., 2018). Our results agree with this finding and showed that both treatments increased their LAI, but transpiration increased most in the NT plot. A consequence of increased transpiration under P limitation is the reduction in WUE.

G_1 and WUE_T showed that WUE increased more in the NPT plot than in the NT plot, even though GPP increased similarly during the spring (Table 4). This is supported by the higher $\delta^{13}C$ at NPT, which indicates that the ratio of leaf-internal CO_2 concentration (c_i) to ambient CO_2 concentration (c_a) is smaller (Cernusak et al., 2013; Seibt et al., 2008). The decrease in the c_i/c_a points toward stronger stomatal closure, less transpiration and thus higher WUE (Medlyn et al., 2011). The increase in WUE at NPT is consistent between methods and across scales that is, $\delta^{13}C$ at leaf level and G_1 and WUE_T at ecosystem scale. This highlights the importance of P availability for WUE across scales.

The N fertilization induced a P limitation in the NT plot and the increasing transpiration might (i) increase P uptake directly via a direct water stream into the plant or by (ii) allowing increased photosynthesis and fueling soil microbes to extract P from organic matter through rhizosphere priming (Kuzyakov, 2002). This is supported by the recent work of Chen et al. (2020), who showed that during the first years following N fertilization, phosphatase activity increases and indicates a progressive attenuation of the N-induced P limitation through the plant and microbial activity. This would also be supported by the increased root biomass at NT (Nair et al., 2019). Additionally, the increased LAI_{green} in the NT plot combined with similar [P] as in CT shows that more P was incorporated into plant material. This additional P at NT must be extracted from the soil or recycled from organic material, maybe through one of the suggested processes.

When sampling the abovementioned differences between treatments at the ecosystem scale, we observed a substantial IAV in WUE and its associated water and carbon fluxes (Figure 4) between dry and wet spring periods (Figure S6). This indicates that ecosystem responses to nutrient availability and stoichiometric imbalance are modulated by water availability. Lower WUE in the NT plot, compared to NPT, resulted in faster senescence toward the end of spring, as shown by Luo et al. (2020). A reduced growing season length and lower WUE (at NT) potentially reduces the carbon uptake compared to an ecosystem losing less water with a higher WUE (NPT). Meteorological drivers, especially the ones related to water availability, strongly impact the productivity of this ecosystem during the spring and winter (El-Madany et al., 2020; Sippel et al., 2017) and influence the phenology of herbaceous plant species at the site (Luo et al., 2018). On top of the IAV, there was a strong seasonal variability with the strongest fertilization effects occurring when conditions were promoting the development of the vegetation (i.e., the winter and spring), while the fertilization effects and their IAV strongly reduce during the summer (Figure 7). This, again, emphasizes that the herbaceous layer drives the fertilization effects rather than the trees, which are the only active component of the ecosystem in the summer and they only have a canopy cover of about 20%. The relationship between LAI_{green} and GPP_{sat} and G_s especially underpin that for low LAI_{green} conditions ($LAI < 0.5\ m^2\ m^{-2}$), the treatment differences are also low.

The strong linear relationship of LAI_{green} to A_{max} and LAI_{green} * [N] to A_{max} suggests that the increased maximum net carbon uptake was driven by increased LAI in both treatments. The effect of nitrogen was through the release of the N limitation which promoted the development of more biomass and potentially, also the increase of chlorophyll content in the leaves. As shown in Luo et al. (2020), the increased biomass development was already happening during the re-greening when the fertilized treatments developed and increased their LAI more rapidly than the CT. This also explains why the largest treatment effects in carbon fluxes were found during the winter and spring periods and emphasize that the study site was N limited.

A positive relationship between leaf nitrogen content and photosynthetic capacity is described at leaf level (Evans, 1989; Kattge et al., 2009) but also at ecosystem scale (Kergoat et al., 2008; Musavi et al., 2016). When using the product of leaf nitrogen content and LAI (i.e., LAI_{green} * [N]) and photosynthetic capacity (i.e., GPP_{sat}) the relationship between LAI_{green} * [N] and GPP_{sat} improves for all treatments (with more explained variance) than that involving only LAI_{green}. The flattening of the curve at higher LAI values could be a consequence of lower leaf levels getting less light. Additionally, leaf properties like the maximum rate of Rubisco carboxylase activity (Vc_{max}) might result in light saturation. This would be in agreement with the relationship of LAI_{green} and LAI_{green} * [N] with G_s, which reached its maximum value of approximately 7 $mm\ s^{-1}$ after LAI_{green} reached approximately 1.0 $m^2\ m^{-2}$. The increase of mean springtime LAI_{green} in the fertilized treatments was approximately 0.7 $m^2\ m^{-2}$, which corresponds with an increase of 40% compared to CT (1.72 $m^2\ m^{-2}$). The reduced evaporation and increased transpiration during spring could be driven by increased LAI because it increases the transpiration-surface per m^2 ground area and additionally intercepts more light which is then not able to heat the soil below the leaves (Pott & Hüppe, 2007; Wei et al., 2017). The surface conductance reaches its maximum already at an LAI of 1.0 $m^2\ m^{-2}$ and at a lower value as compared to GPP_{sat} (1.8 $m^2\ m^{-2}$). With increasing LAI, leaves could start to shade other leaves below, reduce their surface temperature and thus VPD within the herbaceous canopy. Similarly, the increasing LAI results in reduced aerodynamic conductance (Figure S9) which in turn hinders the exchange of moisture out of the canopy and thus potentially reduces VPD. In addition, these processes are modulated by modified WUE as a result of nutrient availability and stoichiometric imbalance of the N:P ratio.

5. Conclusion

Systematic differences in ecosystem responses were detected between NT and NPT as a consequence of nutrient application. The fertilizer application at NT led to a wide N:P ratio (i.e., a stoichiometric imbalance and potential P limitation in the herbaceous layer), which increased transpiration to extract more P from the soil. In addition, springtime biomass production and carbon fluxes increased compared to the control. Altogether, springtime WUE increased in the NT plot, but not as strongly as in the NPT plot, where not only GPP increased but also the transpiration was reduced compared to NT. WUE_T only increased in the NPT plot but decreased in the NT plot.

The functional relationships between LAI_{green} and A_{max} and GPP_{sat} show better fits when using LAI_{green} * [N] and emphasize the importance of [N] for explaining the carbon fluxes, while for G_s using LAI_{green} * [N] even reduced the goodness of fit. A lower N:P ratio at CT and NPT resulted in the lowest surface conductance while it was strongly increased at NT with its high N:P ratio.

Overall, the changes in WUE in the fertilized treatments were first driven by the increase in carbon uptake through increased LAI. Second, between-treatment differences were driven by the narrow N:P ratio in the NPT plot, which reduced transpiration compared to NT and increased WUE. Further, the strength of all responses was highly modulated by water availability. Our results suggest the importance of compensating P limitations in case of N:P imbalance to increase WUE in semi-arid ecosystems.

Data Availability Statement

The half-hourly eddy covariance, meteorological, nutrient, isotopic signatures, and green LAI data are made available via http://doi.org/10.5281/zenodo.4453567 (El-Madany et al., 2021). For the availability of the hyperspectral images we refere to (Pacheco-Labrador et al., 2020) and the data availability statement within.

Acknowledgments
The authors thank Martin Hertel, Kathrin Henkel, Ramón López-Jimenez, Yonatan Cáceres and Enrique Juarez for support during fieldwork and site maintenance. Tarek S. El-Madany, Javier Pacheco-Labrador, Mirco Migliavacca, Markus Reichstein and Oscar Perez-Priego thank the Alexander von Humboldt Stiftung for financial support of the MaNiP project, M. Pilar Martín and Vicente Burchard-Levine thank the Spanish Ministry of Economy and Competitiveness for financing the flights with hyperspectral imagery through the FLUXPEC project (CGL2012-34383) and SynerTGE (CGL2015-G9095-R), and Javier Pacheco-Labrador and Mirco Migliavacca acknowledge the German Aerospace Center (DLR) and the German Federal Ministry of Economic Affairs and Energy that provided support within the framework of the EnMAP project (Contract No. 50EE1621). Victor Rolo was funded by a "*Talento*" fellowship (TA18022) funded by the regional government of Extremadura (Spain). Open access funding enabled and organized by Projekt DEAL.

References

Baret, F., & Buis, S. (2008). Estimating canopy characteristics from remote sensing observations: Review of methods and associated problems. In S. Liang, (Ed.), *Advances in land remote sensing: System, modeling, inversion and application* (pp. 173–201). Springer Netherlands. https://doi.org/10.1007/978-1-4020-6450-0_7

Beer, C. P., Reichstein, M., Baldocchi, D., Law, B. E., & Papale, D. (2009). Temporal and among-site variability of inherent water use efficiency at the ecosystem level. *Global Biogeochemical Cycles*, *23*(2). https://doi.org/10.1029/2008gb003233

Bogdanovich, E., Perez-Priego, O., El-Madany, T. S., Guderle, M., Pacheco-Labrador, J., Levick, S. R., et al. (2021). Using terrestrial laser scanning for characterizing tree structural parameters and their changes under different management in a Mediterranean open woodland. *Forest Ecology and Management*, *486*, 118945. https://doi.org/10.1016/j.foreco.2021.118945

Brand, W. A. (2013). Atomic weights: Not so constant after all. *Analytical and Bioanalytical Chemistry*, *405*(9), 2755–2761. https://doi.org/10.1007/s00216-012-6608-0

Breiman, L. (2001). Random forests. *Machine Learning*, *45*(1), 5–32. https://doi.org/10.1023/a:1010933404324

Brooks, P. D., Geilmann, H., Werner, R. A., & Brand, W. A. (2003). Improved precision of coupled?13C and?15N measurements from single samples using an elemental analyzer/isotope ratio mass spectrometer combination with a post-column six-port valve and selective CO2 trapping; improved halide robustness of the combustion reactor using CeO2. *Rapid Communications in Mass Spectrometry*, *17*(16), 1924–1926. https://doi.org/10.1002/rcm.1134

Casals, P., Gimeno, C., Carrara, A., Lopez-Sangil, L., & Sanz, M. (2009). Soil CO2 efflux and extractable organic carbon fractions under simulated precipitation events in a Mediterranean Dehesa. *Soil Biology and Biochemistry*, *41*(9), 1915–1922. https://doi.org/10.1016/j.soilbio.2009.06.015

Cernusak, L. A., Ubierna, N., Winter, K., Holtum, J. A. M., Marshall, J. D., & Farquhar, G. D. (2013). Environmental and physiological determinants of carbon isotope discrimination in terrestrial plants. *New Phytologist*, *200*(4), 950–965. https://doi.org/10.1111/nph.12423

Cernusak, L. A., Winter, K., & Turner, B. L. (2011). Transpiration modulates phosphorus acquisition in tropical tree seedlings. *Tree Physiology*, *31*(8), 878–885. https://doi.org/10.1093/treephys/tpr077

Chen, J., Groenigen, K. J. van, Hungate, B. A., Terrer, C., Groenigen, J.-W. van, Maestre, F. T., et al. (2020). Long-term nitrogen loading alleviates phosphorus limitation in terrestrial ecosystems. *Global Change Biology*, 5077–5086. https://doi.org/10.1111/gcb.15218

Coplen, T. B. (2011). Guidelines and recommended terms for expression of stable-isotope-ratio and gas-ratio measurement results. *Rapid Communications in Mass Spectrometry*, *25*(17), 2538–2560. https://doi.org/10.1002/rcm.5129

Coskun, D., Britto, D. T., & Kronzucker, H. J. (2016). Nutrient constraints on terrestrial carbon fixation: The role of nitrogen. *Journal of Plant Physiology*, *203*, 95–109. https://doi.org/10.1016/j.jplph.2016.05.016

Cramer, M. D., Hoffmann, V., & Verboom, G. A. (2008). Nutrient availability moderates transpiration inEhrharta calycina. *New Phytologist*, *179*(4), 1048–1057. https://doi.org/10.1111/j.1469-8137.2008.02510.x

Dash, J., & Curran, P. J. (2007). Evaluation of the MERIS terrestrial chlorophyll index (MTCI). *Advances in Space Research*, *39*(1), 100–104. https://doi.org/10.1016/j.asr.2006.02.034

de Vries, W., Solberg, S., Dobbertin, M., Sterba, H., Laubhahn, D., Reinds, G. J., et al. (2008). Ecologically implausible carbon response? *Nature*, *451*(7180), E1–E3. https://doi.org/10.1038/nature06579

Du, E., Terrer, C., Pellegrini, A. F. A., Ahlström, A., van Lissa, C. J., Zhao, X., et al. (2020). Global patterns of terrestrial nitrogen and phosphorus limitation. *Nature Geoscience*, *13*(3), 221–226. https://doi.org/10.1038/s41561-019-0530-4

Legendre, P., & Legendre, L., (Eds.), (1998). Numerical ecology(2nd ed., *24*. Elsevier). https://doi.org/10.1016/S0167-8892(98)80066-3

Ellsworth, D. S., Anderson, I. C., Crous, K. Y., Cooke, J., Drake, J. E., Gherlenda, A. N., et al. (2017). Elevated CO2 does not increase eucalypt forest productivity on a low-phosphorus soil. *Nature Climate Change*, *7*(4), 279–282. https://doi.org/10.1038/nclimate3235

El-Madany, T. S., Carrara, A., Kolle, O., Gerardo, M., Martin, M. P., Gonzalez-Cascon, R., et al. (2021). Data for "How nitrogen and phosphorus availability change water use efficiency in a mediterranean savanna ecosystem" [Data set]. *Zenodo*. https://doi.org/10.5281/zenodo.4453567

El-Madany, T. S., Carrara, A., Martin, M. P., Moreno, G., Kolle, O., Pacheco-Labrador, J., et al. (2020). Drought and heatwave impacts on semi-arid ecosystems' carbon fluxes along a precipitation gradient. *Philosophical Transactions of the Royal Society B: Biological Sciences*, *375*(1810), 20190519–20190527. https://doi.org/10.1098/rstb.2019.0519

El-Madany, T. S., Reichstein, M., Perez-Priego, O., Carrara, A., Moreno, G., Pilar Martín, M., et al. (2018). Drivers of spatio-temporal variability of carbon dioxide and energy fluxes in a Mediterranean savanna ecosystem. *Agricultural and Forest Meteorology*, *262*, 258–278. https://doi.org/10.1016/j.agrformet.2018.07.010

Elser, J. J., Fagan, W. F., Kerkhoff, A. J., Swenson, N. G., & Enquist, B. J. (2010). Biological stoichiometry of plant production: Metabolism, scaling and ecological response to global change. *New Phytologist*, *186*(3), 593–608. https://doi.org/10.1111/j.1469-8137.2010.03214.x

Evans, J. R. (1989). Photosynthesis and nitrogen relationships in leaves of C3 plants. *Oecologia*, *78*(1), 9–19. https://doi.org/10.1007/bf00377192

Fay, P. A., Prober, S. M., Harpole, W. S., Knops, J. M. H., Bakker, J. D., Borer, E. T., et al. (2015). Grassland productivity limited by multiple nutrients. *Nature Plants*, *1*(7), 15080. https://doi.org/10.1038/nplants.2015.80

Fernández-Martínez, M., Vicca, S., Janssens, I. A., Sardans, J., Luyssaert, S., Campioli, M., et al. (2014). Nutrient availability as the key regulator of global forest carbon balance. *Nature Climate Change*, *4*(6), 471–476. https://doi.org/10.1038/nclimate2177

Field, C., Merino, J., & Mooney, H. A. (1983). Compromises between water-use efficiency and nitrogen-use efficiency in five species of California evergreens. *Oecologia*, *60*(3), 384–389. https://doi.org/10.1007/bf00376856

Ford, H., Roberts, A., & Jones, L. (2016). Nitrogen and phosphorus co-limitation and grazing moderate nitrogen impacts on plant growth and nutrient cycling in sand dune grassland. *The Science of the Total Environment*, *542*, 203–209. https://doi.org/10.1016/j.scitotenv.2015.10.089

Fratini, G., & Mauder, M. (2014). Toward a consistent eddy-covariance processing: An intercomparison of EddyPro and TK3. *Atmospheric Measurement Techniques*, *7*(7), 2273–2281. https://doi.org/10.5194/amt-7-2273-2014

Grünzweig, J. M., Lin, T., Rotenberg, E., Schwartz, A., & Yakir, D. (2003). Carbon sequestration in arid-land forest. *Global Change Biology*, *9*(5), 791–799. https://doi.org/10.1046/j.1365-2486.2003.00612.x

Güsewell, S. (2004). N:P ratios in terrestrial plants: Variation and functional significance. *New Phytologist*, *164*(2), 243–266. https://doi.org/10.1111/j.1469-8137.2004.01192.x

Han, J., Chen, J., Miao, Y., & Wan, S. (2016). Multiple Resource Use Efficiency (m RUE): A new concept for ecosystem production. *Scientific Reports*, *6*(1), 37453. https://doi.org/10.1038/srep37453

Hersbach, H., Bell, B., Berrisford, P., Biavati, G., Horanyi, A., Munoz Sabater, J., et al. (2018). ERA5 hourly data on single levels from 1979 to present. *Copernicus Climate Change Service (C3S) Climate Data Store (CDS)*. https://doi.org/10.24381/cds.adbb2d47

Homolová, L., Malenovský, Z., Clevers, J. G. P. W., García-Santos, G., & Schaepman, M. E. (2013). Review of optical-based remote sensing for plant trait mapping. *Ecological Complexity*, *15*, 1–16. https://doi.org/10.1016/j.ecocom.2013.06.003

Huang, G., Hayes, P. E., Ryan, M. H., Pang, J., & Lambers, H. (2017). Peppermint trees shift their phosphorus-acquisition strategy along a strong gradient of plant-available phosphorus by increasing their transpiration at very low phosphorus availability. *Oecologia*, *185*(3), 387–400. https://doi.org/10.1007/s00442-017-3961-x

Huang, Z., Liu, B., Davis, M., Sardans, J., Peñuelas, J., & Billings, S. (2015). Long-term nitrogen deposition linked to reduced water use efficiency in forests with low phosphorus availability. *New Phytologist*, *210*(2), 431–442. https://doi.org/10.1111/nph.13785

Jiang, M., Caldararu, S., Zaehle, S., Ellsworth, D. S., & Medlyn, B. E. (2019). Toward a more physiological representation of vegetation phosphorus processes in land surface models. *New Phytologist*, *222*(3), 1223–1229. https://doi.org/10.1111/nph.15688

Joffre, R. (1990). Plant and soil nitrogen dynamics in mediterranean grasslands: A comparison of annual and perennial grasses. *Oecologia*, *85*(1), 142–149. https://doi.org/10.1007/bf00317355

Kattge, J., Knorr, W., Raddatz, T., & Wirth, C. (2009). Quantifying photosynthetic capacity and its relationship to leaf nitrogen content for global-scale terrestrial biosphere models. *Global Change Biology*, *15*(4), 976–991. https://doi.org/10.1111/j.1365-2486.2008.01744.x

Kergoat, L., Sébastien, L., Almut, A., Le, D., Valérie, & Bernard, S. (2008). Nitrogen controls plant canopy light-use efficiency in temperate and boreal ecosystems. *Journal of Geophysical Research*, *113*, G04017. https://doi.org/10.1029/2007jg000676

Kljun, N., Calanca, P., Rotach, M. W., & Schmid, H. P. (2015). A simple two-dimensional parameterization for Flux Footprint Prediction (FFP). *Geoscientific Model Development*, *8*(11), 3695–3713. https://doi.org/10.5194/gmd-8-3695-2015

Klodd, A. E., Nippert, J. B., Ratajczak, Z., Waring, H., & Phoenix, G. K. (2016). Tight coupling of leaf area index to canopy nitrogen and phosphorus across heterogeneous tallgrass prairie communities. *Oecologia*, *182*(3), 889–898. https://doi.org/10.1007/s00442-016-3713-3

Knauer, J., El-Madany, T. S., Zaehle, S., & Migliavacca, M. (2018). Bigleaf—An R package for the calculation of physical and physiological ecosystem properties from eddy covariance data. *PloS One*, *13*(8), e0201114. https://doi.org/10.1371/journal.pone.0201114

Knauer, J., Zaehle, S., Medlyn, B. E., Reichstein, M., Williams, C. A., Migliavacca, M., et al. (2018). Toward physiologically meaningful water-use efficiency estimates from eddy covariance data. *Global Change Biology*, *24*, 694–710. https://doi.org/10.1111/gcb.13893

Kröbel, R., Campbell, C. A., Zentner, R. P., Lemke, R., Steppuhn, H., Desjardins, R. L., & De Jong, R. (2012). Nitrogen and phosphorus effects on water use efficiency of spring wheat grown in a semi-arid region of the Canadian prairies. *Canadian Journal of Soil Science*, *92*(4), 573–587. https://doi.org/10.4141/cjss2011-055

Kuzyakov, Y. (2002). Review: Factors affecting rhizosphere priming effects. *Zeitschrift für Pflanzenernährung und Bodenkunde*, *165*(4), 382–396. https://doi.org/10.1002/1522-2624(200208)165:4<382::AID-JPLN382>3.0.CO;2-#

Lasslop, G., Reichstein, M., Papale, D., Richardson, A. D., Arneth, A., Barr, A., et al. (2010). Separation of net ecosystem exchange into assimilation and respiration using a light response curve approach: Critical issues and global evaluation. *Global Change Biology*, *16*(1), 187–208. https://doi.org/10.1111/j.1365-2486.2009.02041.x

Legendre, P. (2018). *Model II regression*. Retrieved from https://cran.r-project.org/web/packages/lmodel2/lmodel2.pdf

Li, Y., Niu, S., & Yu, G. (2016). Aggravated phosphorus limitation on biomass production under increasing nitrogen loading: A meta-analysis. *Global Change Biology*, *22*(2), 934–943. https://doi.org/10.1111/gcb.13125

Liang, X., Zhang, T., Lu, X., Ellsworth, D. S., BassiriRad, H., You, C., et al. (2020). Global response patterns of plant photosynthesis to nitrogen addition: A meta-analysis. *Global Change Biology*, *26*, 3585–3600. https://doi.org/10.1111/gcb.15071

Lloyd, J., & Taylor, J. A. (1994). On the Temperature Dependence of Soil Respiration. *Functional Ecology*, *8*(3), 315. https://doi.org/10.2307/2389824

Luo, Y., El-Madany, T., Ma, X., Nair, R., Jung, M., Weber, U., et al. (2020). Nutrients and water availability constrain the seasonality of vegetation activity in a Mediterranean ecosystem. *Global Change Biology*, *26*(8), 4379–4400. https://doi.org/10.1111/gcb.15138

Luo, Y., El-Madany, T. S., Filippa, G., Ma, X., Ahrens, B., Carrara, A., et al. (2018). Using near-infrared-enabled digital repeat photography to track structural and physiological phenology in mediterranean tree-grass ecosystems. *Remote Sensing*, *10*(8), 1293. https://doi.org/10.3390/rs10081293

Luyssaert, S., Jammet, M., Stoy, P. C., Estel, S., Pongratz, J., Ceschia, E., et al. (2014). Land management and land-cover change have impacts of similar magnitude on surface temperature. *Nature Climate Change*, *4*(5), 389–393. https://doi.org/10.1038/nclimate2196

Magill, A. H., Aber, J. D., Currie, W. S., Nadelhoffer, K. J., Martin, M. E., McDowell, W. H., et al. (2004).Ecosystem response to 15 years of chronic nitrogen additions at the Harvard Forest LTER, Massachusetts, USA, *Forest Ecology and Management*. *196*(1). 7–28. https://doi.org/10.1016/j.foreco.2004.03.033

Magnani, F., Mencuccini, M., Borghetti, M., Berbigier, P., Berninger, F., Delzon, S., et al. (2007). The human footprint in the carbon cycle of temperate and boreal forests. *Nature*, *447*(7146), 849–851. https://doi.org/10.1038/nature05847

Magnani, F., Mencuccini, M., Borghetti, M., Berninger, F., Delzon, S., Grelle, A., et al. (2008). Magnani et al. reply. *Nature*, *451*(7180), E3–E4. https://doi.org/10.1038/nature0657810.1038/nature06580

Maire, V., Wright, I. J., Prentice, I. C., Batjes, N. H., Bhaskar, R., van Bodegom, P. M., et al. (2015). Global effects of soil and climate on leaf photosynthetic traits and rates. *Global Ecology and Biogeography*, *24*(6), 706–717. https://doi.org/10.1111/geb.12296

Masek, J. G., Vermote, E. F., Saleous, N. E., Wolfe, R., Hall, F. G., Huemmrich, K. F., et al. (2006). A Landsat surface reflectance dataset for North America, 1990-2000. *IEEE Geoscience and Remote Sensing Letters*, *3*(1), 68–72. https://doi.org/10.1109/lgrs.2005.857030

Mauder, M., & Foken, T. (2011). *Documentation and instruction manual of the eddy-covariance software package TK3*, p. 60

Medlyn, B. E., De Kauwe, M. G., Lin, Y.-S., Knauer, J., Duursma, R. A., Williams, C. A., et al. (2017). How do leaf and ecosystem measures of water-use efficiency compare? *New Phytologist*, *216*(3), 758–770. https://doi.org/10.1111/nph.14626

Medlyn, B. E., Duursma, R. A., Eamus, D., Ellsworth, D. S., Prentice, I. C., Barton, C. V. M., et al. (2011). Reconciling the optimal and empirical approaches to modeling stomatal conductance. *Global Change Biology*, *17*(6), 2134–2144. https://doi.org/10.1111/j.1365-2486.2010.02375.x

Meinshausen, N. (2006). Quantile Regression Forests. *Journal of Machine Learning Research*, *7*, 17.

Migliavacca, M., Perez-Priego, O., Rossini, M., El-Madany, T. S., Moreno, G., van der Tol, C., et al. (2017). Plant functional traits and canopy structure control the relationship between photosynthetic CO2 uptake and far-red sun-induced fluorescence in a Mediterranean grassland under different nutrient availability. *New Phytologist*, *214*, 1078–1091. https://doi.org/10.1111/nph.14437

Morris, K. A., Nair, R. K. F., Moreno, G., Schrumpf, M., & Migliavacca, M. (2019). Fate of N additions in a multiple resource-limited Mediterranean oak savanna. *Ecosphere*, *10*(11), e02921. https://doi.org/10.1002/ecs2.2921

Muggeo, V. M. R. (2003). Estimating regression models with unknown break-points. *Statistics in Medicine*, *22*(19), 3055–3071. https://doi.org/10.1002/sim.1545

Muggeo, V. M. R. (2017). Interval estimation for the breakpoint in segmented regression: A smoothed score-based approach. *Australian & New Zealand Journal of Statistics*, *59*(3), 311–322. https://doi.org/10.1111/anzs.12200

Musavi, T., Mahecha, M. D., Migliavacca, M., Reichstein, M., van de Weg, M. J., van Bodegom, P. M., et al. (2015). The imprint of plants on ecosystem functioning: A data-driven approach. *International Journal of Applied Earth Observation and Geoinformation*, *43*, 119–131. https://doi.org/10.1016/j.jag.2015.05.009

Musavi, T., Migliavacca, M., van de Weg, M. J., Kattge, J., Wohlfahrt, G., van Bodegom, P. M., et al. (2016). Potential and limitations of inferring ecosystem photosynthetic capacity from leaf functional traits. *Ecology and Evolution*, *6*(20), 7352–7366. https://doi.org/10.1002/ece3.2479

Nair, R. K. F., Morris, K. A., Hertel, M., Luo, Y., Moreno, G., Reichstein, M., et al. (2019). N : P stoichiometry and habitat effects on Mediterranean savanna seasonal root dynamics. *Biogeosciences*, *16*(9), 1883–1901. https://doi.org/10.5194/bg-16-1883-2019

Nelson, J. A. (2020). TranspirationEstimationAlgorithm: Addition of DOI tag. *Zenodo*. https://doi.org/10.1037/e508932020-001

Nelson, J. A., Carvalhais, N., Cuntz, M., Delpierre, N., Knauer, J., Ogée, J., et al. (2018). coupling water and carbon fluxes to constrain estimates of transpiration: The TEA algorithm. *Journal of Geophysical Research Biogeoscience*, *123*(12), 3617–3632. https://doi.org/10.1029/2018jg004727

Oldroyd, G. E. D., & Leyser, O. (2020). A plant's diet, surviving in a variable nutrient environment. *Science*, *368*(6486), eaba0196. https://doi.org/10.1126/science.aba0196

Pacheco-Labrador, J., El-Madany, T., Martín, M., Migliavacca, M., Rossini, M., Carrara, A., & Zarco-Tejada, P. J. (2017). Spatio-temporal relationships between optical information and carbon fluxes in a mediterranean tree-grass ecosystem. *Remote Sensing*, *9*(6), 608. https://doi.org/10.3390/rs9060608

Pacheco-Labrador, J., El-Madany, T. S., Martin, M. P., Gonzalez-Cascon, R., Carrara, A., Moreno, G., et al. (2020). Combining hyperspectral remote sensing and eddy covariance data streams for estimation of vegetation functional traits. *Biogeosciences Discussions*, 1–38. https://doi.org/10.5194/bg-2019-501

Pang, J., Zhao, H., Bansal, R., Bohuon, E., Lambers, H., Ryan, M. H., & Siddique, K. H. M. (2018). Leaf transpiration plays a role in phosphorus acquisition among a large set of chickpea genotypes. *Plant, Cell and Environment*, *41*(9), 2069–2079. https://doi.org/10.1111/pce.13139

Papale, D., Reichstein, M., Aubinet, M., Canfora, E., Bernhofer, C., Kutsch, W., et al. (2006). Toward a standardized processing of Net Ecosystem Exchange measured with eddy covariance technique: Algorithms and uncertainty estimation. *Biogeosciences*, *3*(4), 571–583. https://doi.org/10.5194/bg-3-571-2006

Peñuelas, J., Canadell, J. G., & Ogaya, R. (2010). Increased water-use efficiency during the 20th century did not translate into enhanced tree growth. *Global Ecology and Biogeography*, *20*(4), 597–608. https://doi.org/10.1111/j.1466-8238.2010.00608.x

Peñuelas, J., Poulter, B., Sardans, J., Ciais, P., Velde, M. van der, Bopp, L., et al. (2013). Human-induced nitrogen–phosphorus imbalances alter natural and managed ecosystems across the globe. *Nature Communications*, *4*, 2934. https://doi.org/10.1038/ncomms3934

Penuelas, J., Janssens, I. A., Ciais, P., Obersteiner, M., & Sardans, J. (2020). Anthropogenic global shifts in biospheric N and P concentrations and ratios and their impacts on biodiversity, ecosystem productivity, food security, and human health. *Global Change Biology*, *26*(4), 1962–1985. https://doi.org/10.1111/gcb.14981

Perez-Priego, O., El-Madany, T. S., Migliavacca, M., Kowalski, A. S., Jung, M., Carrara, A., et al. (2017). Evaluation of eddy covariance latent heat fluxes with independent lysimeter and sapflow estimates in a Mediterranean savannah ecosystem. *Agricultural and Forest Meteorology*, *236*, 87–99. https://doi.org/10.1016/j.agrformet.2017.01.009

Pott, R., & Hüppe, J. (2007). *Spezielle Geobotanik: Pflanze - klima - Boden ; mit 31 Tabellen*. Springer.

R Development Core Team. (2015). *R: A language and environment for statistical computing*. Retrieved from URL: https://www.R-project.org/

Reichstein, M., Bahn, M., Mahecha, M. D., Kattge, J., & Baldocchi, D. D. (2014). Linking plant and ecosystem functional biogeography. *Proceedings of the National Academy of Sciences*, *111*(38), 13697–13702. https://doi.org/10.1073/pnas.1216065111

Reichstein, M., Falge, E., Baldocchi, D., Papale, D., Aubinet, M., Berbigier, P., et al. (2005). On the separation of net ecosystem exchange into assimilation and ecosystem respiration: Review and improved algorithm. *Global Change Biology*, *11*(9), 1424–1439. https://doi.org/10.1111/j.1365-2486.2005.001002.x

Riginos, C. (2009). Grass competition suppresses savanna tree growth across multiple demographic stages. *Ecology*, *90*(2), 335–340. https://doi.org/10.1890/08-0462.1

Rivest, D., Rolo, V., López-Díaz, M. L., & Moreno, G. (2011). Belowground competition for nutrients in shrub-encroached Mediterranean dehesas. *Nutrient Cycling in Agroecosystems*, *90*(3), 347–354. https://doi.org/10.1007/s10705-011-9436-2

Rolo, V., & Moreno, G. (2012). Interspecific competition induces asymmetrical rooting profile adjustments in shrub-encroached open oak woodlands. *Trees*, *26*(3), 997–1006. https://doi.org/10.1007/s00468-012-0677-8

Rose, L., Buitenwerf, R., Cramer, M., February, E. C., & Higgins, S. I. (2018). Effects of nutrient supply on carbon and water economies of C4 grasses. *Functional Plant Biology*, *45*(9), 935. https://doi.org/10.1071/fp17359

Rouse, J. W., Haas, R. H., Schell, J. A., & Deering, D. W. (1974). *Monitoring vegetation systems in the great plains with ERTS*. Retrieved from https://ntrs.nasa.gov/search.jsp?R=19740022614

Sankaran, M., Ratnam, J., & Hanan, N. P. (2004). Tree-grass coexistence in savannas revisited - Insights from an examination of assumptions and mechanisms invoked in existing models. *Ecology Letters*, *7*(6), 480–490. https://doi.org/10.1111/j.1461-0248.2004.00596.x

Scalon, M. C., Haridasan, M., & Franco, A. C. (2017). Influence of long-term nutrient manipulation on specific leaf area and leaf nutrient concentrations in savanna woody species of contrasting leaf phenologies. *Plant and Soil*, *421*(1–2), 233–244. https://doi.org/10.1007/s11104-017-3437-0

Scholes, R. J., & Archer, S. R. (1997). Tree-grass interactions in savannas. *Annual Review of Ecology and Systematics*, *28*(1), 517–544. https://doi.org/10.1146/annurev.ecolsys.28.1.517

Seibt, U., Rajabi, A., Griffiths, H., & Berry, J. A. (2008). Carbon isotopes and water use efficiency: Sense and sensitivity. *Oecologia*, *155*(3), 441. https://doi.org/10.1007/s00442-007-0932-7

Sippel, S., El-Madany, T. S., Migliavacca, M., Mahecha, M. D., Carrara, A., Flach, M., et al. (2017). Warm winter, wet spring, and an extreme response in ecosystem functioning on the Iberian Peninsula. *Bulletin of the American Meteorological Society*, *98*(12). Chapter 16. https://doi.org/10.1175/BAMS-D-17-0135.1

Thom, A. S. (1972). Momentum, mass and heat exchange of vegetation. *Quarterly Journal of the Royal Meteorological Society*, *98*(415), 124–134. https://doi.org/10.1002/qj.49709841510

Wei, Z., Yoshimura, K., Wang, L., Miralles, D. G., Jasechko, S., & Lee, X. (2017). Revisiting the contribution of transpiration to global terrestrial evapotranspiration. *Geophysical Research Letters*, *44*(6), 2792–2801. https://doi.org/10.1002/2016gl072235

Werner, R. A., & Brand, W. A. (2001). Referencing strategies and techniques in stable isotope ratio analysis. *Rapid Communications in Mass Spectrometry*, *15*(7), 501–519. https://doi.org/10.1002/rcm.258

Werner, R. A., Bruch, B. A., & Brand, W. A. (1999). ConFlo III - an interface for high precision δ13C and δ15N analysis with an extended dynamic range. *Rapid Communications in Mass Spectrometry*, *13*(13), 1237–1241. https://doi.org/10.1002/(sici)1097-0231(19990715)13:13<1237::aid-rcm633>3.0.co;2-c

Wicklein, H. F., Ollinger, S. V., Martin, M. E., Hollinger, D. Y., Lepine, L. C., Day, M. C., et al. (2012). Variation in foliar nitrogen and albedo in response to nitrogen fertilization and elevated CO2. *Oecologia*, *169*(4), 915–925. https://doi.org/10.1007/s00442-012-2263-6

Wutzler, T., Lucas-Moffat, A., Migliavacca, M., Knauer, J., Sickel, K., Šigut, L., et al. (2018). Basic and extensible post-processing of eddy covariance flux data with REddyProc. *Biogeosciences*, *15*(16), 5015–5030. https://doi.org/10.5194/bg-15-5015-2018

Wutzler, T., Perez-Priego, O., Morris, K., El-Madany, T., & Migliavacca, M. (2019). Soil CO2 efflux errors are log normally distributed - Implications and guidance. *Geoscientific Instrumentation, Methods and Data Systems Discussions*, *1–19*. https://doi.org/10.5194/gi-2019-10

Zhou, S., Yu, B., Huang, Y., & Wang, G. (2014). The effect of vapor pressure deficit on water use efficiency at the subdaily time scale. *Geophysical Research Letters*, *41*(14), 5005–5013. https://doi.org/10.1002/2014gl060741

Zhu, J., Wang, Q., He, N., Smith, M. D., Elser, J. J., Du, J., et al. (2016). Imbalanced atmospheric nitrogen and phosphorus depositions in China: Implications for nutrient limitation. *Journal of Geophysical Research Biogeoscience*, *121*(6), 1605–1616. https://doi.org/10.1002/2016jg003393